DETERMINATION OF LONGWAVE IRRADIANCE AT THE GROUND

by
WILLIAM JAMES BLACKBURN, B.A.

A THESIS SUBMITTED TO THE
SCHOOL OF GRADUATE STUDIES IN
PARTIAL FULFILMENT OF THE
REQUIREMENT FOR THE DEGREE
MASTER OF SCIENCE

McMASTER UNIVERSITY
APRIL 1980

DETERMINATION OF LONGWAVE IRRADIANCE AT THE GROUND

MASTER OF SCIENCE (1980)
(GEOGRAPHY)

McMASTER UNIVERSITY
HAMILTON, ONTARIO

TITLE: DETERMINATION OF LONGWAVE IRRADIANCE AT THE GROUND

AUTHOR: WILLIAM JAMES BLACKBURN, B.A. (McMaster)

ADVISOR: DR. JOHN A. DAVIES

NUMBER OF PAGES: xii; 76.

ABSTRACT

Incoming longwave irradiance at the earth's surface under cloudless or near cloudless skies was determined by three instrumental methods. The most reasonable results were obtained using a Eppley pyrgeometer fitted with a silicon dome. Problems associated with an Eppley pyrgeometer equipped with a KRS-5 dome and with a Funk-type Swissteco pyrradiometer are demonstrated. Measured irradiances were compared with those calculated from various physical and empirical models under a variety of atmospheric conditions. The former usually agreed with measured irradiance to within 15%. The latter showed variable agreement. The Swinbank model with only one dependent variable provided as good an estimate as the more complex physical models. The role of aerosol at infrared wavelengths is examined and is shown to have minimal effect on the longwave flux at the ground.

ACKNOWLEDGEMENTS

The author wishes to express his appreciation to Dr. John A. Davies for his scholarly expertise and continued interest and direction in the preparation of this thesis. I am also indebted to Dr. Wayne R. Rouse for his assistance in the measurement program in the sub-arctic and for the advice and encouragement that he has given me during my graduate studies. Thanks is also extended to Mr. Terry Dwyer and his staff of the Mount Hope Weather Office for providing surface weather record data and Buffalo radiosonde profiles used in the model calculations. The research was supported by grants from the National Research Council.

TABLE OF CONTENTS

LIST OF FIGURES

LIST OF TABLES

LIST OF SYMBOLS

I_{bv} spectral blackbody emittance

I_v spectral blackbody intensity at wavenumber ν

K_v absorption coefficient

$K\downarrow$ solar irradiance

$K\uparrow$ outgoing solar radiation

L longwave irradiance

L_B calculated longwave irradiance using the Brunt equation

L_{IJ} calculated longwave irradiance using the Idso-Jackson equation

L_{IND} measured longwave irradiance at an industrial site

L_{KRS-5} measured longwave irradiance using the KRS-5 domed pyrgeometer

L_{RE} measured longwave irradiance at a residential site

L_{RES} measured longwave irradiance by residual

L_{SIL} measured longwave irradiance using the silicon-domed pyrgeometer

$L_{SWIN(1)}$ calculated longwave irradiance using the Swinbank model uncorrected for cloud and time of day

$L_{SWIN(2)}$ calculated longwave irradiance using the Swinbank model corrected for cloud and time of day

$L\uparrow$ outgoing longwave radiation

P atmospheric pressure

P_o standard surface pressure

Q_{abs} efficiency factor for absorption

Q_{ext} efficiency factor for total extinction

Q_{sca} efficiency factor for scattering

$Q\downarrow$	total incoming irradiance
Q^*	net radiation
T	air temperature
T_c	blackbody cavity temperature
e	vapour pressure
g	acceleration due to gravity
h	scale height
m	complex index of refraction
n_{IM}	imaginary part of complex index of refraction
n_{RE}	real part of complex index of refraction
$n(r)$	particle size distribution
n^l	gas concentration
q	specific humidity
r	particle radius
r_c	modal radius
u	optical pathlength
u_c	carbon dioxide pathlength
u_{o_3}	ozone pathlength
u_w	water vapour pathlength
u^l	scaled optical pathlength
v	wavenumber
w	single scattering albedo
x	Mie size parameter
β	aerosol bulk extinction coefficient

δe	carbon dioxide-water vapour overlap correction
ε_f	flux emissivity
ε_g	layer emissivity containing trace gases
λ	wavelength
μ	cosine of angle of incidence
ρ	air density
σ	Stefan-Boltzmann constant
τ	optical-depth
ψ	transmissivity
ω	solid angle

CHAPTER I

INTRODUCTION

A. Aims of Study

Studies in radiation climatology within Canada have focused primarily on solar irradiance which is monitored routinely by the Atmospheric Environment Service (AES) at several locations across the country. Longwave irradiance, however, has not been measured anywhere in Canada on a routine basis. In fact, for North America, aside from the Canadian measurements made during the International Field Year for the Great Lakes (IFYGL), longwave irradiance data remain scarce. Furthermore experimental studies by Enz et al. (1974) and Albrecht and Cox (1977) have shown that measured values, by the Eppley pyrgeometer, the only commercially available sensor which measures the irradiance directly, are of questionable accuracy. Alternative measurement methods include direct measurement with a newer version of the Eppley pyrgeometer equipped with a silicon dome, residual determinations from measurements of other radiation fluxes and estimates from models. The data base against which models can be tested is very limited however.

This study will examine the performance of two flux emissivity models, SANDJ and ELDOWN: the former employing the temperature-dependent

emissivities of Staley and Jurica (1970) and the latter using temperature-independent emissivities of Kuhn (1963) and three empirical models (Brunt, 1932; Swinbank, 1963 and Idso-Jackson, 1969) and results of various instrumental determinations of irradiance. These data were collected largely at Hamilton, Ontario under cloudless or near cloudless skies. Smaller data sets of three days each were obtained at Churchill, Manitoba and at the Canada Centre for Inland Waters (CCIW), Burlington, Ontario. For simplicity, measurements were restricted to cloudless days.

The primary aims of the study are: (1) to determine the relative performance of sensors that are commonly used to measure longwave irradiance, (2) to examine the performance of selected models and (3) to assess the role of aerosol in the infrared.

B. Previous work

Enz et al. (1975) have studied the performance of the Eppley KRS-5 domed pyrgeometer. They showed that the dome absorbs solar radiation and radiates as an extraneous longwave source to the sensing thermopile. Measured values obtained under cloudless skies exceeded calculated values derived from empirical formulae by 11-20%. Longwave radiation varied with solar irradiance when the test was repeated under partial cloud. A ventilation system which provided a constant air flow across the dome was effective in reducing fluctuations caused by varying wind speeds. The dome also weathers when exposed

to the atmosphere (Davies and Schertzer, 1974), so that its transmission properties may change over time.

Albrecht and Cox (1977) identified three major sources of error with this model of pyrgeometer. These are, battery voltage uncertainties, non-linearities in circuitry at extreme temperatures and differential heating of the instrument. A reduction of irradiance values by $22 Wm^{-2}$ was recommended to correct for solar heating of the dome.

The residual method, employing a Funk-type radiometer fitted with a blackbody cavity, also possesses uncertainties as outlined by Robinson et al., (1972) who noted rapid fluctuations in cavity temperature attributed to convection. In this study, the cavity was insulated from solar radiation by embedding it in styrofoam. In a study using shipboard sensors, Polavarapu (1978) compared measurements from two matched Funk net pyrradiometers mounted on either side of a ship with a single Funk pyrradiometer. Excellent agreement was found between the two approaches, although the former method provided slightly higher daytime values.

The performance of empirical models has been examined by Swinbank (1963), Monteith (1964), Deacon (1970), Paltridge (1970) and Idso (1972, 1974). The temperature-based models of Swinbank (1963) and Idso-Jackson (1969) were compared with pyrradiometric measurements by Idso (1974) in a study at Phoenix, Arizona. Calculations using the Brunt (1932) temperature and vapour pressure dependent equation were also performed. The Swinbank and Idso-Jackson models yielded similar results for air temperatures

above freezing, but the former under-estimated measured irradiance at air temperatures below freezing.

Kuhn et al. (1974) have tested their model RADIANCE. Calculations were performed for cloudless and cloudy skies using Buffalo radiosonde profiles. Excellent agreement was found between calculated and observed irradiances. Davies and Uboegbulam (1978) have shown that the flux emissivity approach (similar to ELDOWN in this study) and the Paltridge (1970) model estimated daily totals of longwave radiation to within 4% of measured values obtained during GATE.

CHAPTER II

THEORETICAL BACKGROUND

A. Transfer Equation for Incoming Irradiance

Longwave irradiance is a function of the amounts, temperature and the absorption and emission properties of the atmospheric constituents. Amounts and temperatures are derived from vertical soundings while absorption properties of gases are usually taken from laboratory determinations.

A detailed derivation and solution of the radiative transfer equation is given in Appendix A. The extinction of radiation due to scattering in the earth's atmosphere is small in comparison with the extinction due to absorption, and as a result the scattering of longwave radiation is often neglected altogether (Ramanathan and Coakley, 1978). Hence, the spectral longwave intensity at the earth's surface is given by

$$\mu \frac{dI_\nu}{d\tau_\nu} = I_{b\nu}(\tau_\nu) - I_\nu(\tau_\nu) \qquad (1)$$

where I_ν = spectral radiation intensity at wavenumber ν
$I_{b\nu}$ = spectral blackbody emittance
μ = cosine of the angle of incidence

The term τ_v is the optical depth defined as

$$\tau_v = \int \rho K_v \, dz \tag{2}$$

where ρ is the density of the gas, and K_v is the absorption coefficient. Equation (1) is readily solved to yield the incoming intensity at τ_o, the optical depth at an arbitrary height. The solution can be written as

$$I_v(\tau_o) = \int_{\tau_1}^{\tau_o} I_{bv} \, e^{-(\tau_o - \tau^1)/\mu} \frac{d\tau^1}{\mu} \tag{3}$$

Hence, the intensity is the sum of contributions from all layers between the top of the atmosphere and the reference level, each attenuated according to its optical distance $(\tau^1 - \tau_o)$ from τ_o. Irradiance is obtained by multiplying by μ and then integrating over wavenumber ν and solid angle ω:

$$L(\tau_o) = \int_{\nu_1}^{\nu_2} d\nu \int_0^{2\pi} \int_{\tau_1}^{\tau_o} I_{bv} \, \mu e^{-(\tau_o - \tau^1)/\mu} \frac{d\tau^1}{\mu} \, d\omega \tag{4}$$

Introducing polar spherical coordinates and the exponential integral as shown in Appendix A, equation (4) can be expressed in terms of flux transmissivity ψ, a function of pathlength u and temperature T $\psi(u - u_o, T)$. The spectral longwave flux density now becomes

$$L(u_o) = \int_{\nu_1}^{\nu_2} d\nu \int_{u}^{\mu o} B_\nu \frac{d\psi}{du}(u - u_o, T)\, du \qquad (5)$$

where $B_\nu = \pi I_{b\nu}$.

Figure 1 shows the absorption spectra of the major atmospheric gases. Water vapour (H_2O) and carbon dioxide (CO_2) are the major absorbers, while ozone (O_3), methane (CH_4) and nitrous oxide (N_2O) are less significant. At wavelengths outside the atmospheric window (8 μm < λ > 13 μm), the atmosphere is virtually a blackbody. Little is known about the effects of aerosols (liquid and solid particulates suspended in the atmosphere) in the infrared. From Mie theory, the aerosol optical depth can be written as

$$\tau_\nu = \int_0^z dz \int_{r_1}^{r_2} \pi r^2 Q_{ext}(x, m)\, n(r)\, dr \qquad (6)$$

where r is particle radius, n(r) is the particle size distribution, and Q_{ext} is the efficiency factor for extinction; the sum of the efficiency factors for absorption Q_{abs} and scattering Q_{sca}. The Mie size parameter x is given by

$$x = \frac{2\pi r}{\lambda} \qquad (7)$$

and the complex index of refraction m is

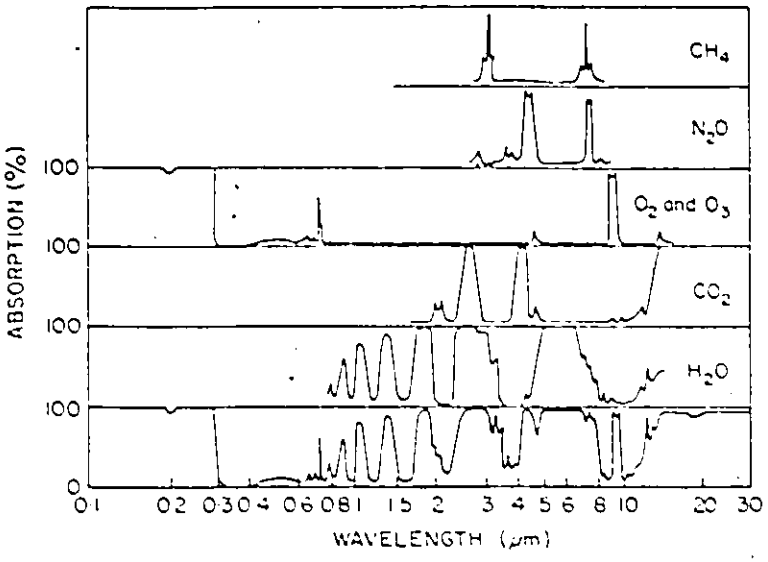

Figure 1: Absorption spectra for important atmospheric gases, with the total absorption described by the lowest curve. (From S.J. Williamson, 1973).

$$m = n_{RE} - i\, n_{IM} \tag{8}$$

This index consists of a real component n_{RE} commonly set equal to 1.5 and an imaginary component n_{IM}; i is $\sqrt{-1}$. The value of n_{IM} determines the absorption characteristics of the particle, if $n_{IM}=0$, the particle does not absorb.

B. Flux Emissivity Models

(i) Formulation

In the flux emissivity approach, equation (5) is re-formulated to eliminate the integration over wavenumber. The emissivity of an arbitrary isothermal atmospheric layer may be defined as the ratio of the total radiative flux emitted through one boundary to the blackbody flux at the same temperature:

$$\varepsilon_f(u - u_o, T) = \frac{1}{\sigma T^4} \int_{\nu_1}^{\nu_2} B_\nu [1 - \tau(u - u_o, T)] d\nu \tag{9}$$

or as

$$\sigma T^4 \varepsilon_f(u - u_o, T) = \int_{\nu_1}^{\nu_2} B_\nu \, d\nu - \int_{\nu_1}^{\nu_2} B_\nu \, \tau(u - u_o, T) \, d\nu \tag{10}$$

Differentiating (5) and (9) with respect to pathlength

$$\frac{dL}{du} = - \int_{\nu_1}^{\nu_2} B_\nu \frac{d\psi}{du} (u - u_o, T)\, d\nu \qquad (11)$$

and

$$\sigma T^4 \frac{d\varepsilon_f}{du} (u - u_o, T) = - \int_{\nu_1}^{\nu_2} B_\nu \frac{d\psi}{du} (u - u_o, T)\, d\nu \qquad (12)$$

Hence,

$$\frac{dL}{du} = \sigma T^4 \frac{d\varepsilon_f}{du} (u - u_o, T) \qquad (13)$$

and

$$L = \int \sigma T^4 \frac{d\varepsilon_f}{du} (u - u_o, T)\, du \qquad (14)$$

Integration over wavenumber is avoided by employing bulk transmissions.

Two FEM's have been used in this study. Both are modified versions by J.A. Davies of a model developed by Dr. Kuhn of the Atmospheric Physics and Chemistry Laboratory, NOAA, Boulder, Colorado. The original model RADVERS was designed to calculate upward, downward and net longwave radiation, cooling rates at various levels in the atmosphere from pressure, temperature and specific humidity data measured by radiosonde. Aerosol can be included in the model by defining the pressure at the top and base of the aerosol layer and the bulk extinction coefficient β. The top of the model atmosphere is assigned a pressure

of 0.1kPa and a temperature of -273°C to establish a zero downward flux. Specific humidity at the top of the atmosphere is zero. Using a band model approach, the relative contributions of the minor absorbers (not included in the FEM's) to the flux at the ground were assessed. The profile for April 18, 1979 was used and calculations showed that for a flux of 214.3 Wm^{-2}, O_3 contributed 3.14 Wm^{-2} (1.47%) and the other trace gases CH_4 and N_2O contributed less; 1.23 Wm^{-2} (0.58%) and 0.8 Wm^{-2} (0.37%). Hence, the contribution due to ozone was assumed trivial and was neglected.

(ii) ELDOWN

The first model, ELDOWN, is a modified version of RADVERS which calculates only the incoming longwave flux; the input data remaining unchanged. ELDOWN employs the empirically-derived emissivities of Kuhn (1963) calculated from in situ, nocturnal radiometersonde measurements of outgoing longwave radiation, air temperature, atmospheric pressure and relative humidity under cloudless skies with little or no ozone. Emissivities are expressed as a function of pressure or optical path but are independent of temperature.

In the formulation of water vapour and carbon dioxide pathlengths, the model accounts for the temperature and pressure dependence of transmittance along any path in the atmosphere using a scaled optical pathlength u^1 defined by

$$u' = u\left(\frac{T_o}{\bar{T}}\right)^{\alpha} \left(\frac{\bar{P}}{P_o}\right)^{\beta'}, \qquad (15)$$

where $\bar{T}$ and $\bar{P}$ are mean layer temperature and pressure, T_o and P_o are standard temperature and pressure for sea level, $\alpha = 0.5$ and $\beta' = 0.12221 + \bar{P}(0.001777 - 0.00000105\bar{P})$. The depth of water vapour u_w is obtained from

$$u_w = \frac{1}{g} \int_{P_1}^{P_2} q \, dp \simeq \frac{1}{g} \sum_{i=1}^{n} \bar{q} \, \Delta P, \qquad (16)$$

where g is acceleration due to gravity (9.81 ms^{-2}) and $\bar{q}$ is mean specific humidity of the layer. The depth of carbon dioxide u_c is calculated from

$$u_c = \frac{n'}{10^6} \frac{h}{P_o} \int_{P_1}^{P_2} dp \qquad (17)$$

where n' is the gas concentration (approximately 300ppm), h is the scale height and P_o = 101.3 kPa. This depth is also corrected for pressure and temperature using $\alpha = 0.5$ and $\beta = 0.6$.

Model calculations were performed according to the scheme shown in Figure 2 where n levels (in this case 7) are defined by radiosonde data (pressure, temperature and specific humidity) creating n-1 layers. These data are used to calculate the blackbody radiation B at each level. Starting at the base of the atmosphere B_7 is calculated from the mean temperature of the layer and the emissivity contribution of the layer $\Delta\varepsilon$ due to the increment of emitter quantity Δu. $\Delta\varepsilon$ is the sum of contri-

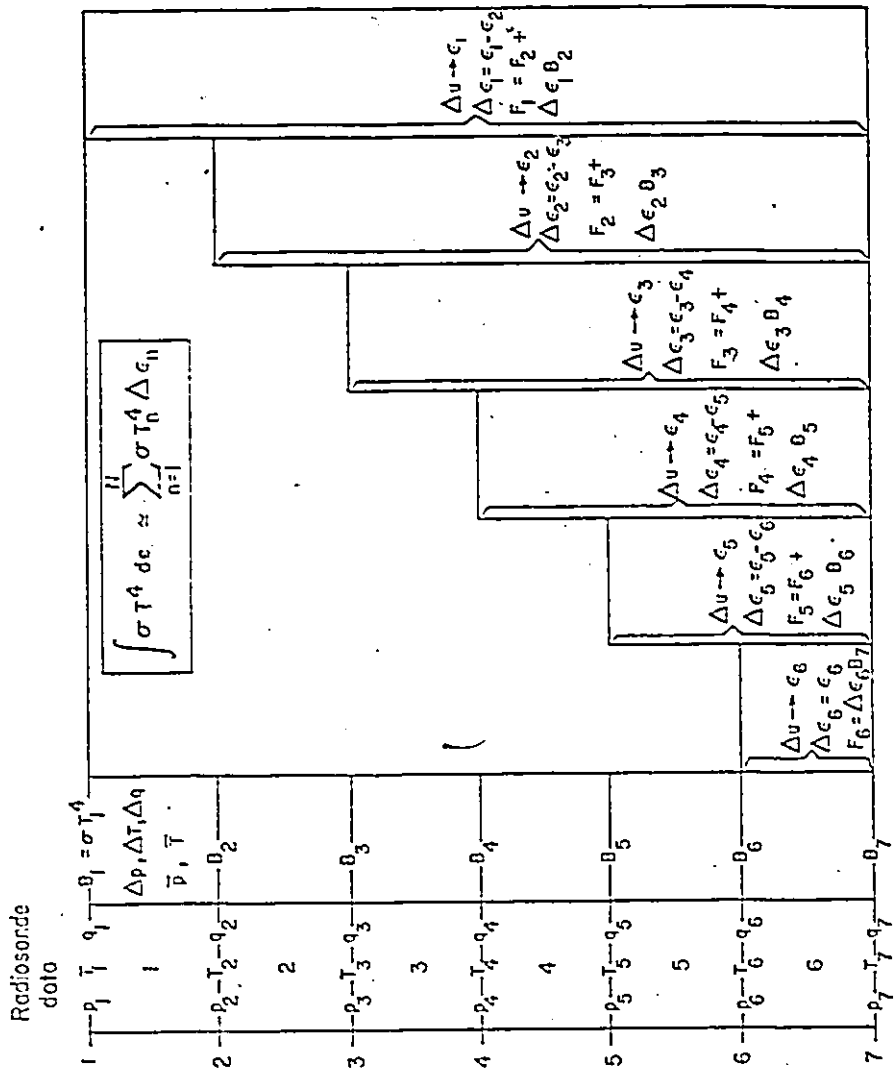

Figure 2: Schematic diagram of the Flux Emissivity Model (J.A. Davies, unpublished).

butions from H_2O, CO_2 and O_3. The flux from the layer is evaluated by $F_6=\Delta\varepsilon_6 B_7$. For subsequent layers, a similar procedure applies.

Kuhn (1963) minimized the effects of H_2O - CO_2 overlap in the 15 μm region by reducing the flux emissivities for CO_2 by 20% over the 14 - 24 μm waveband. It is assumed that emission from CO_2 and H_2O may be added together without serious error.

(iii) SANDJ

The second FEM, SANDJ, is computationally similar to ELDOWN but employs the temperature-dependent emissivities tabulated by Staley and Jurica (1970) which were calculated from the laboratory-derived flux transmissivities and generalized absorption coefficients of Elsasser and Culbertson (1960).

Staley and Jurica corrected for overlap by CO_2 and H_2O in the 13-15 μm band as follows. Let

$$\varepsilon(u_w, u_c, T) = \frac{1}{\sigma T^4} \int_{13\ \mu m}^{1mm} [1 - \psi(u_w - u_{wo}, T)\ \psi(u_c - u_{co}, T)]\sigma T^4\, d\varepsilon. \qquad (18)$$

Expanding the transmission function in the manner

$$1 - \psi_1\psi_2 = (1 - \psi_1) + (1 - \psi_2) - (1 - \psi_1)(1 - \psi_2), \qquad (19)$$

$$\varepsilon(u_w, u_c, T) = \frac{1}{\sigma T^4} \int_{\varepsilon_1}^{\varepsilon_2} [1 - \psi(u_w - u_{wo}, T)] \sigma T^4 d\varepsilon + \frac{1}{\sigma T^4} \int_{\varepsilon_1}^{\varepsilon_2} [1 - \psi(u_c - u_{co}, T)] \sigma T^4 d\varepsilon - \frac{1}{\sigma T^4} \int_{\varepsilon_1}^{\varepsilon_2} [1 - \psi(u_w - u_{wo}, T)] [1 - \psi(u_c - u_{co}, T)] \sigma T^4 d\varepsilon \quad (20)$$

where u_w and u_c are the water vapour and carbon dioxide pathlengths. Staley and Jurica (1970) note that since O_3 emission is small and does not overlap with that of H_2O or CO_2, it could be added directly. The total emissivity is defined as

$$\varepsilon(u_w, u_c, T) = \varepsilon(u_w, T) + \varepsilon(u_c, T) + \varepsilon(u_{c_3}, T) - \delta e \quad (21)$$

where δe is the overlap correction which they have tabulated. Equation (5) is evaluated numerically from

$$L(u_o) = [[1 - \sum_{i=2}^{n} \Delta\varepsilon_i (u_w) - \sum_{i=2}^{n} \Delta\varepsilon_i(u_c) + \sum_{i=2}^{n} \delta\varepsilon_i (u_w, u_c, T)] \sigma T^4(\tau_1)] + \sum_{i=2}^{n} \sigma \bar{T}^4 \Delta\varepsilon_i(u_w) + \sum_{i=2}^{n} \sigma \bar{T}^4 \Delta\varepsilon_i(u_c) - \sum_{i=2}^{n} \sigma \bar{T}^4 \delta\varepsilon_i(u_w, u_c, T) \quad (22)$$

where the square-bracketed terms apply to the boundary of the system and the remaining terms apply to the atmospheric layers.

C. Empirical Models

Early work by Brunt (1932) related longwave irradiance to screen level temperature and vapour pressure e by

$$L = a + b\sqrt{e}\ \sigma T^4 \qquad (23)$$

where a and b are empirical constants which vary with geographic site and σ is the Stefan-Boltzmann constant.

Swinbank (1963) fitted nocturnal measurements of L with

$$L = 5.31 \times 10^{-13}\ T^6 \qquad (24)$$

which is air temperature dependent only. Testing the hypothesis that "within the range of humidity that occurs in the atmosphere, incoming longwave radiation is a function of screen level temperature alone", a regression analysis showed that L is strongly dependent on T and largely independent of e. Log plots of L against T revealed that the former was not truly a function of T^4, but rather T^6.

Paltridge (1970) questioned whether the Swinbank model was appropriate for daytime applications since it was derived using nocturnal data. The Swinbank model was shown to over-estimate L

in the early afternoon. Paltridge (1970) and Idso (1972) both argued that using screen level temperature in calculations of atmospheric radiation may cause fluxes to be under-estimated at night and over-estimated during the day. The use of the temperature of the "centre of gravity" of the atmosphere at a height of about 200-300m is favoured.

The Idso-Jackson (1969) model is expressed by

$$L = \sigma T^4 [1 - c \exp [-d(273 - T)^2]] \qquad (25)$$

where c and d are empirical constants. Idso (1974) compared Idso-Jackson model estimates with those of the Swinbank model and with residual measurements. Results showed notable seasonal differences. Equation (25) under-estimated measured values in the early morning and over-estimated at all other times during the day. The Swinbank model severely under-estimated when $T < 0^oC$ but agreed well with measured values when $T > 0^oC$. Idso suggests that models which depend only on temperature do not perform as well as those which rely on both T and e.

CHAPTER III

EXPERIMENTAL PROCEDURES

A. Methods

Longwave irradiance L was obtained by direct measurement or as a residual from other irradiance measurements. Direct measurements were made with two Eppley pyrgeometers. Since L can be calculated from either

$$L = Q\downarrow - K\downarrow \tag{26}$$

or

$$L = Q^* - K\downarrow + K\uparrow + L\uparrow \tag{27}$$

residual estimates were obtained from both equations where $Q\downarrow$ is total (solar plus longwave) irradiance, $K\downarrow$, Q^*, $K\uparrow$ and $L\uparrow$ the incoming solar, net, reflected solar and outgoing longwave irradiances respectively.

B. Measurement

(i) Solar irradiance

An Eppley precision spectral pyranometer was used to measure solar irradiance. This sensor comprises a circular, wirewound multi-junction Eppley thermopile, coated with Parson's black laquer (non-wavelength-selective absorption). A pair of removable precision ground and polished hemispheres of Schott optical glass protect the thermopile surface and exclude longwave radiation.

(ii) Longwave irradiance

Two Eppley precision pyrgeometers similar in design to the precision spectral pyranometer were used to measure L directly. A circuit compensates for the longwave irradiance that the cold junctions of the thermopile receives from the body of the instrument. This latter irradiance is assumed to be that for a blackbody at the thermopile temperature. A thermistor senses thermopile temperature.

One sensor was fitted with a KRS-5 dome and the other with a silicon dome. Following tests at Atmospheric Environment Service by J.R. Latimer, Davies and Schertzer (1974) reported that the Eppley KRS-5 dome contains a filter which is hygroscopic and oxidizes upon exposure to the atmosphere. The sensor dome becomes discoloured and the longwave transmissivity of the dome decreases with age. A modified version of this sensor replaces the KRS-5 dome with a silicon dome. The latter is characterized by a vacuum-deposited

interference filter on the dome's inner surface which isolates the terrestrial longwave radiation from solar shortwave radiation in the daytime. The composite transmission of the pyrgeometer is about 4 - 50 μm.

At the end of the study period the Eppley silicon-domed pyrgeometer was re-calibrated by the AES using two different calibration procedures. The first was carried out in a blackbody chamber used to calibrate net radiometers where the sensor views an entire hemisphere, while the second procedure allows the sensor to see only a cone of radiation. Calibration factors were 2% and 6% smaller than the manufacturer's. Since the second procedure is similar to that used by Eppley Laboratories, the calibration using that method was adopted, bearing in mind that the fluxes could be as much as 4% greater than they are if the calibration factor from the first procedure had been used. It is noteworthy that the AES have found a similar discrepancy between the manufacturer's calibration and their own for other pyrgeometers, but that these two calibrating procedures should yield similar answers.

At the Churchill site, residual estimates of L were obtained using both equations (26) and (27). For convenience, these will be referred to as the Q↓ and Q* methods. Q* was measured with a Funk-type net radiometer (Swissteco). This sensor comprises two polyethelene hemispheres which transmit all wavelengths. The domes were inflated and purged with dried air pumped through silica gel

using an aquarium pump. For the Q↓ method, L was obtained from two Funk-type radiometers converted to pyrradiometers by replacing the lower polyethelene hemispheres with a blackbody cavity. In an attempt to determine solar effects on cavity temperature one cavity was exposed to the atmosphere while the other was submerged in a styrofoam mount covered with mylar reflective tape. The sensor signal is proportional to the difference between incoming total irradiance and the longwave irradiance from the cavity. The latter term is calculated from the Stefan-Boltzmann law

$$L\uparrow = \varepsilon \sigma T_c^4 \quad , \tag{28}$$

where ε = emissivity (assumed to be unity), σ is the Stefan-Boltzmann constant and T_c is the cavity temperature obtained using an imbedded thermocouple referenced to a thermostatically controlled ice point unit. The incoming irradiance is then obtained by adding the black-body irradiance corresponding to the cavity temperature.

At both the Hamilton and Burlington sites, residual estimates were obtained using the Q↓ method. During winter, when air temperatures were often less than $0^{\circ}C$ considerable problems arose in the measurement of longwave irradiance by the residual method. The battery-driven aquarium pumps used to keep the pyrradiometer domes inflated often froze and had to be replaced with electrically-driven pumps. This

ensured a continuous air flow. Since the ice point unit (frigister) is designed to bring the reference temperature down to $0^{o}C$, uncertainties in the reference temperature became a problem when air temperatures were below freezing. Attempts to solve this problem included the substitution of different alcohol-water solutions, but this approach was neither satisfactory nor efficient. The frigister was then re-instated and placed in a well ventilated, insulated wooden box with a built in heat source (40W light bulb). Frequent checks were made to ensure no over-heating. Several days of data were discarded during this experimental period whenever the reference temperature was uncertain. An accurate cavity temperature is crucial since the blackbody flux from the cavity is a major term in the calculation of irradiance using this method. A platinum resistance thermometer was used as a check on the ice point unit temperature. This approach proved to be the best method, since whenever the reference temperature deviated from zero, a correction could be applied to the signal before the flux from the cavity was calculated.

The recording of data posed as many problems as the measurements themselves. Methods of recording data ranged from manual recording using a Keithley potentiometer, an Esterline Angus strip chart recorder and an automatic Esterline Angus D2020 data logger to a Solartron electronic data logger with magnetic tape recording. Each sensor signal was sampled every fifteen or twenty minutes. This scanning

interval was thought to be appropriate since changes in longwave irradiance over time are small. In all cases, a measuring system zero was established.

C. Sites and Data Collection

Measurements were made under cloudless skies, or when the atmosphere was judged to be nearly cloudless on the basis of the solar radiation record and the surface weather records. Measurements at a field station approximately 14 km east of Churchill, Manitoba (58° 45'N, 94° 5'W) over the period August 23-25, 1978 provided data using both residual techniques. The measurement program was expanded to include pyrgeometer measurements from roof-top sites at McMaster University, Hamilton (43° 20'N, 79° 50'W) from February 13 - April 12, 1979 and at the Canada Centre for Inland Waters (CCIW), Burlington for selected days in May 1979. Additional longwave irradiance measurements were obtained at McMaster using the silicon-domed pyrgeometer from June to November, 1979.

For the flux emissivity models radiosonde ascents (0000Z and 1200Z) from the Churchill Upper Air Station were used to obtain pressure, dry bulb temperature and dewpoint depression at different levels in the atmosphere. Buffalo (approximately 100 km south-east of Hamilton) radiosonde ascents (1200Z and 2300Z) were used for the McMaster and CCIW sites. Surface weather records from the Churchill Upper Air Station and Mount Hope Airport (14.5 km south of the McMaster site) provided daily cloud information and air temperatures.

CHAPTER IV

INTERCOMPARISON OF INSTRUMENTAL DETERMINATIONS OF LONGWAVE IRRADIANCE

A. Eppley Pyrgeometers

Daytime data from the KRS-5 sensor contain errors due to solar heating of the dome as discussed by Enz et al. (1975). This is demonstrated in Figure 3 which shows the results of simultaneous measurements with all sensors (October 31) and in Figure 4 (March 19) where the two Eppley pyrgeometers are compared. Daytime values from the KRS-5 domed sensor show a greater increase during periods of intense solar radiation than those from a similar sensor equipped with a silicon dome. At night, the two sets of measurements agree more closely. Similar trends were observed in the data of March 20 and 21. The KRS-5 sensor may provide acceptable nocturnal irradiance estimates, but it may over-estimate by as much as 24% during the day. Further justification of this claim is presented in the discussion to follow where results from these sensors are compared with those from the residual method.

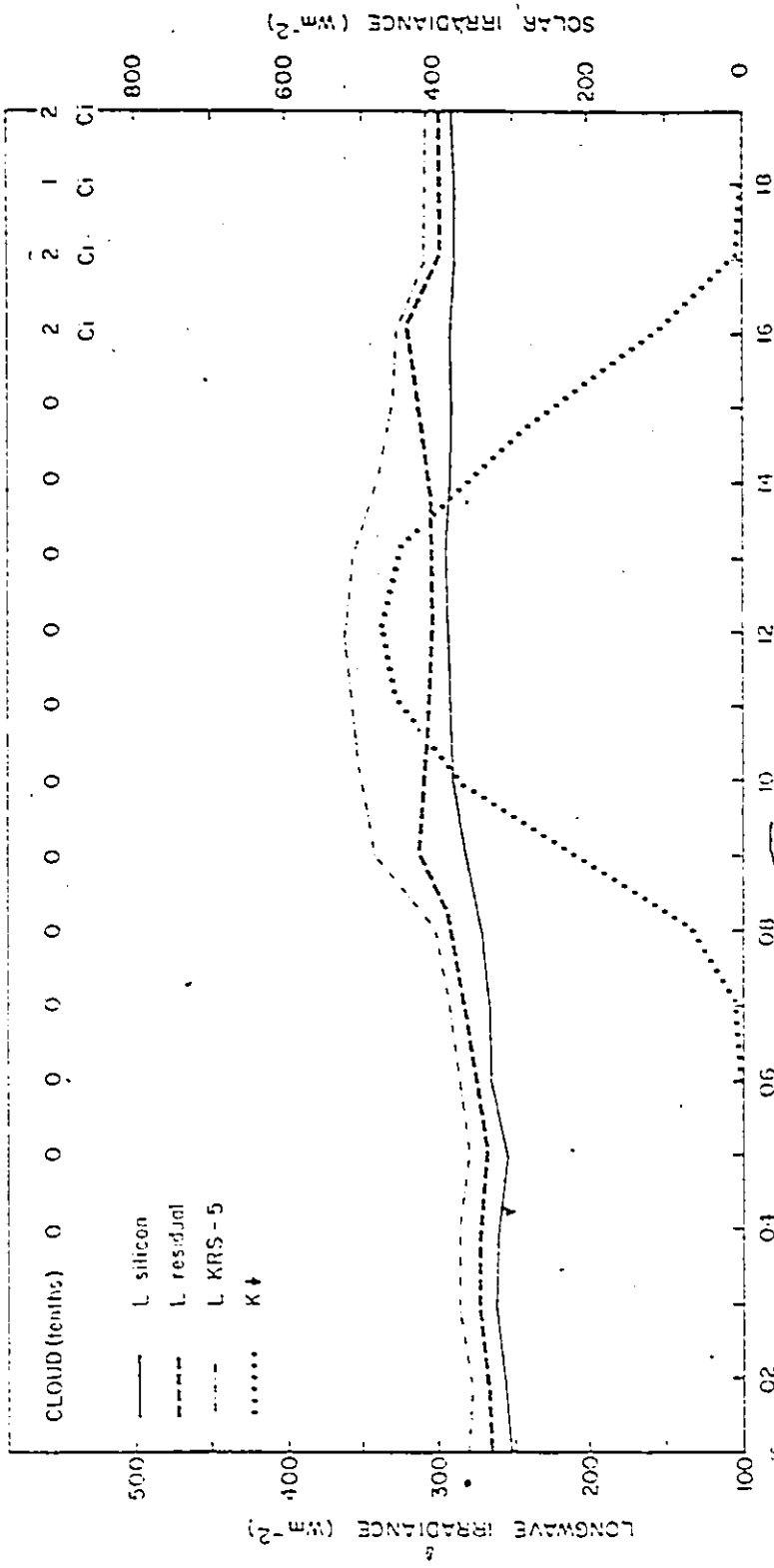

Figure 3: Longwave irradiance measurements by all three instrumental methods for October 31, 1979.

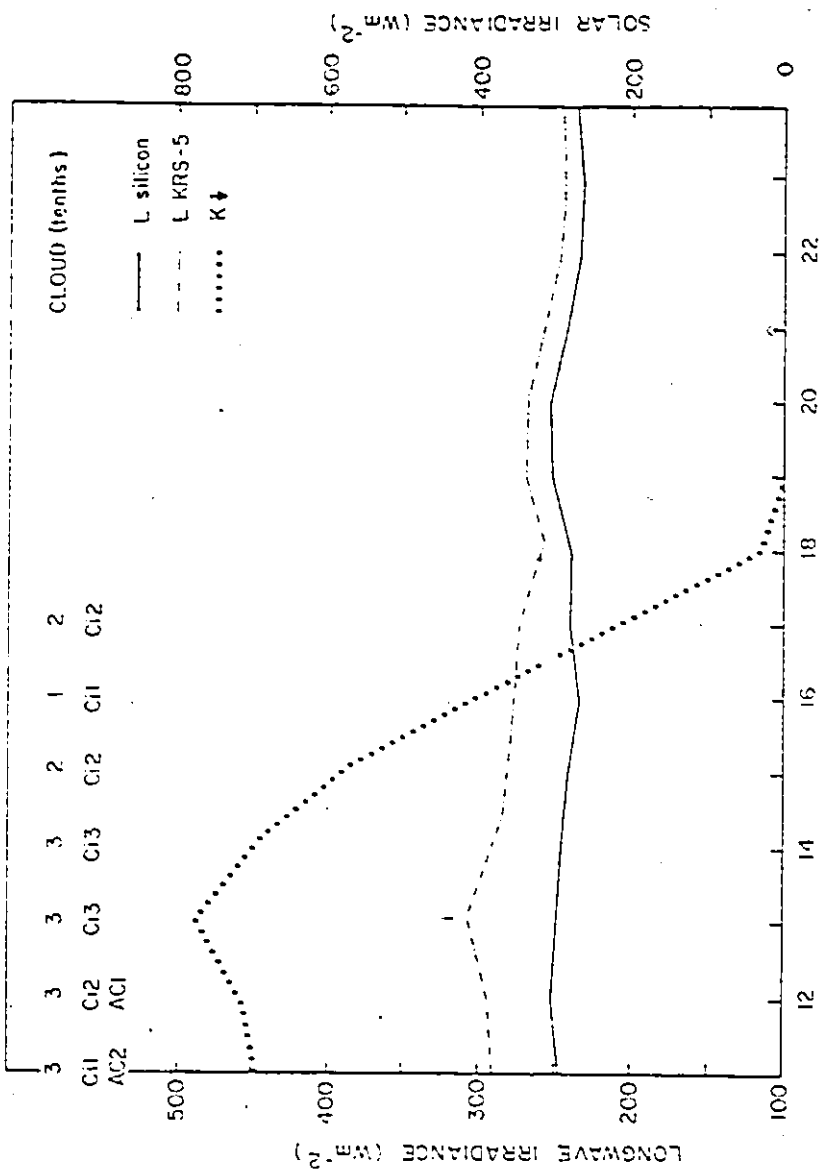

Figure 4: Longwave irradiance from the two Eppley pyrgeometers for March 19, 1979.

B. Pyrgeometers and pyrradiometers

Data collected under nearly cloudless skies on April 18, 1979 (Figure 5) were used to compare silicon dome estimates with those from the Q↓ method. Irradiance values using a pyrradiometer submerged in a styrofoam mount were found to agree to within 3% with silicon-dome measurements at night. These differences are considered to lie within the accuracy of the radiometer. These data show however, that anomalous increases in Swissteco values occur immediately following sunrise and preceeding sunset. Swissteco measurements exceeded silicon irradiance measurements by a maximum of 21% ($50 Wm^{-2}$) in the morning and 16% ($44 Wm^{-2}$) in the early evening. The Swissteco sensor may have under-estimated the solar components during these two periods. According to the manufacturer, the cosine response of the Swissteco is within $\pm 3\%$ for zenith angles 0^{o} - 70^{o}. It is unknown for larger angles. Both of the pyrradiometers used to obtain these data were recalibrated for shortwave radiation at the AES and tests showed that calibration factors were only marginally different (1% and 3%) from the manufacturer's original values. Field experiments carried out by the AES suggests that the behaviour of the Swissteco sensor is still not fully understood and several problems remain to be solved. In the analysis of measurements obtained at McMaster, it is hypothesized that these sensors may significantly under-estimate solar irradiance at high zenith angles and then the residual method would over-estimate the longwave component. This may account for anomalous peaks in irradiance near sunrise and sunset (Figures 3 and 5). The

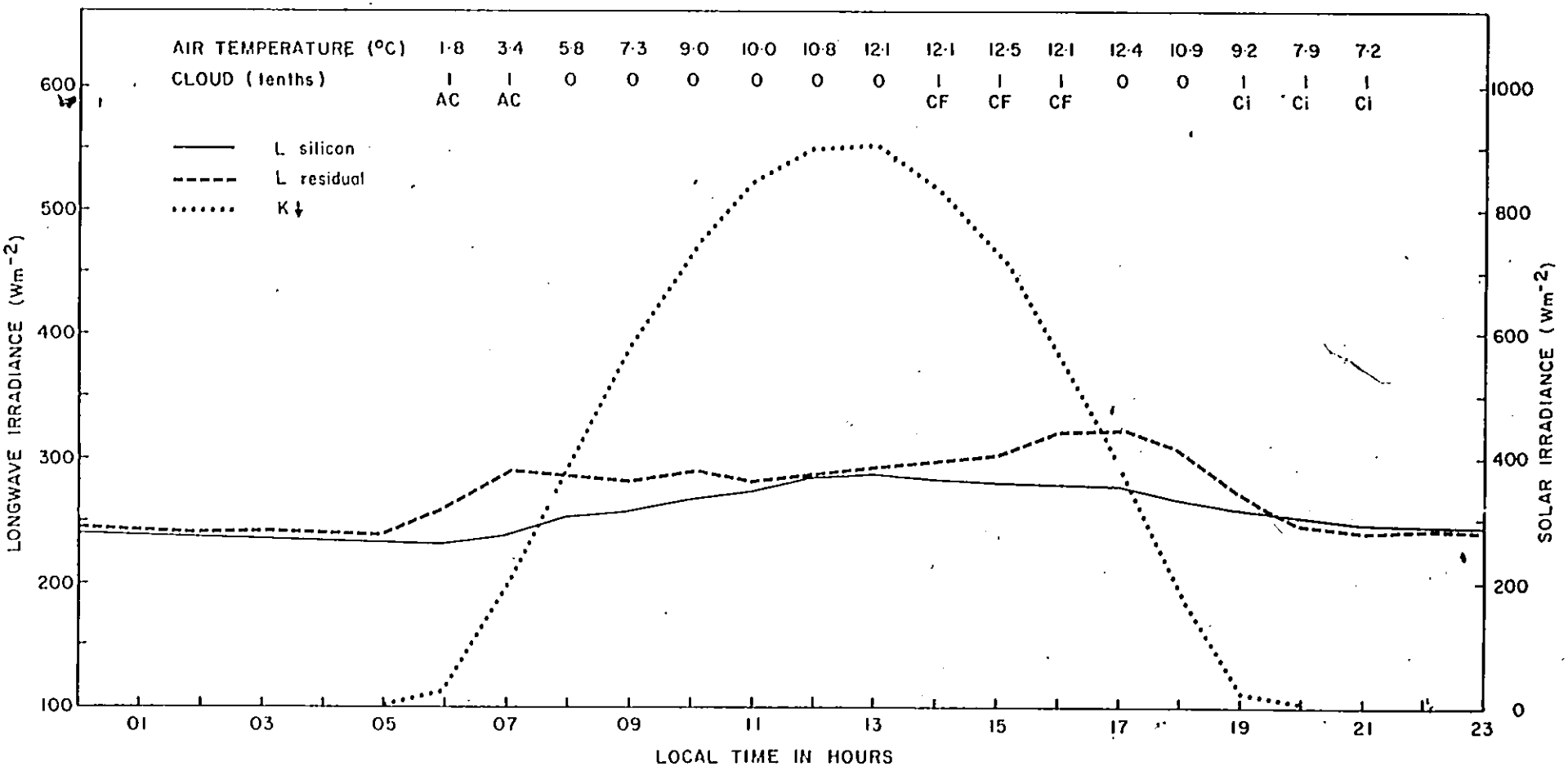

Figure 5: Longwave irradiance from the Eppley silicon-domed pyrgeometer and the Swissteco pyrradiometer for April 18, 1979.

residual values also exhibit a slight decrease around mid-day. This phenomenon suggests a decrease either in atmospheric emissivity or radiating temperature, neither of which seems to be physically justified. Similar phenomena using the residual method are apparent in Canadian results during GATE (Uboegbulam, 1978).

On April 11, 1979 an experiment was performed to assess the solar effect. Data shown in Figure 6 were collected under two distinct cloud regimes. Between 0600 and 1200 local time, cloud fields of 3/10 - 5/10 cirrus were reported, while 10/10 stratocumulus/altocumulus were dominant over the period 1300 - 1800. Similar patterns to other days occurred in the data up to 1200 local time with the peak in longwave irradiance following sunrise as shown in Figure 6. Following this, longwave irradiance values increased in response to overcast skies despite the reduction in both air temperature and solar irradiance. The peak in Swissteco-derived irradiances prior to sunset did not occur. These data suggest that the expected under-estimation of solar irradiance near sunset was modified by clouds obscuring the sun.

C. Comparison of pyrradiometer estimates

In response to questions posed by Robinson, Davies and Nunez (1972) during IFYGL, notably the effect of solar radiation on blackbody cavity temperature, two Swissteco pyrradiometers were used in this study

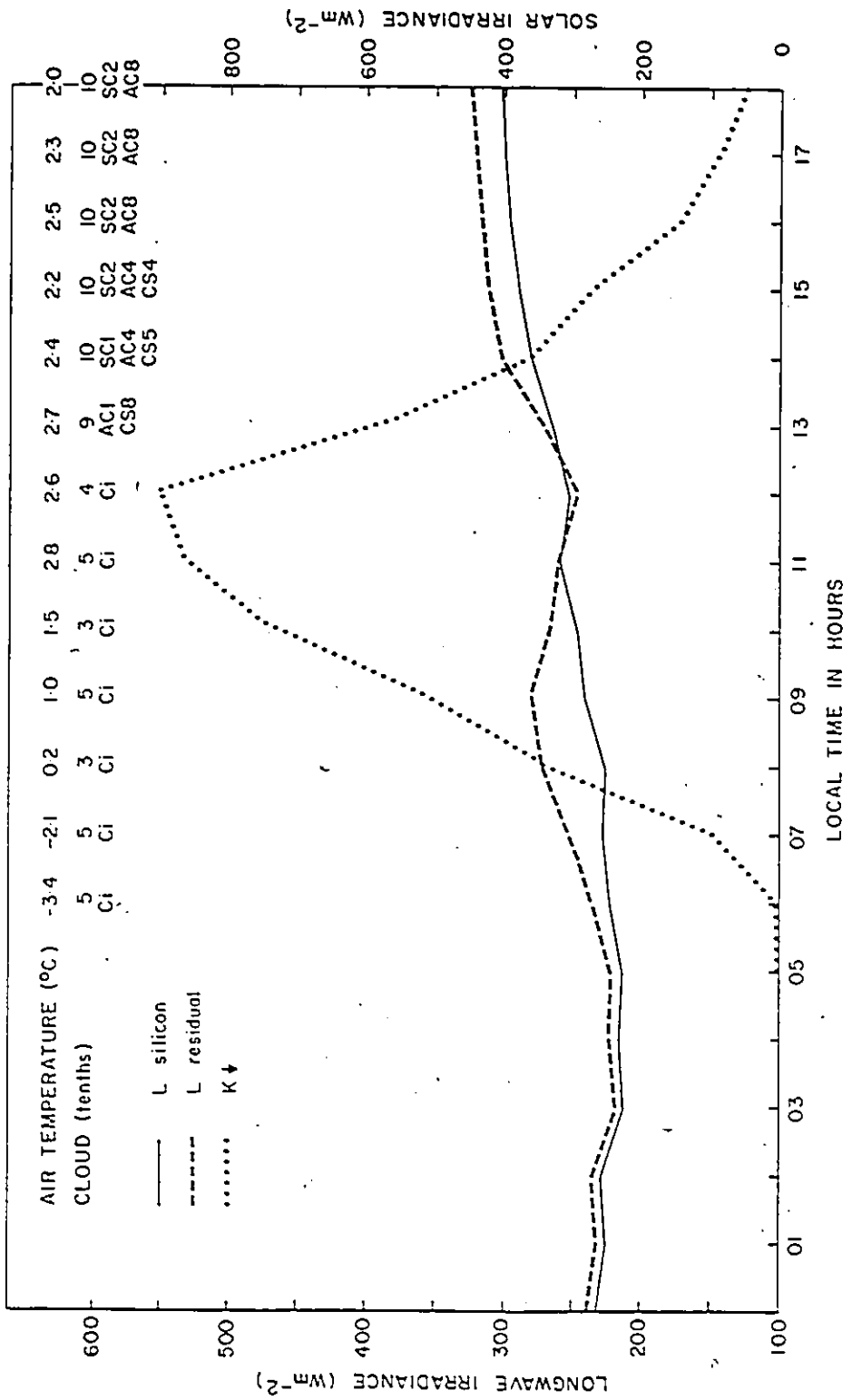

Figure 6: Performance of the pyrradiometer under partly cloudy and overcast skies. April 11, 1979.

to determine longwave irradiance estimates from the Q↓ method. One pyrradiometer was set up with the blackbody cavity exposed to the atmosphere while the second sensor's cavity was mounted in a styrofoam base. In principle, any difference between the two pyrradiometer estimates of Q↓ can be expressed by relating the total sensor signal Q↓ to the incoming radiation Q uncorrected for temperature and the cavity emittance σT_c^4 (^oK). The styrofoam mount was ineffective in reducing solar heating effects. An expected "flattening out" of the cavity temperature curve for the styrofoam mounted pyrradiometer did not occur. Both temperature curves were found to peak during periods of intense solar radiation. Differences between the two temperature curves were insignificant.

D. Q* and Q↓ methods

. Data collected at Churchill, Manitoba over the period 1100 August 23 to 1200 August 25 (Figure 7) show good agreement (usually within $10 Wm^{-2}$) between longwave irradiance values obtained using both the Q* and Q↓ methods. The Q* method shares problems common to the Q↓ method. Additional error may arise from an increase in the number of independent measurements required to arrive at the residual estimate of longwave irradiance.

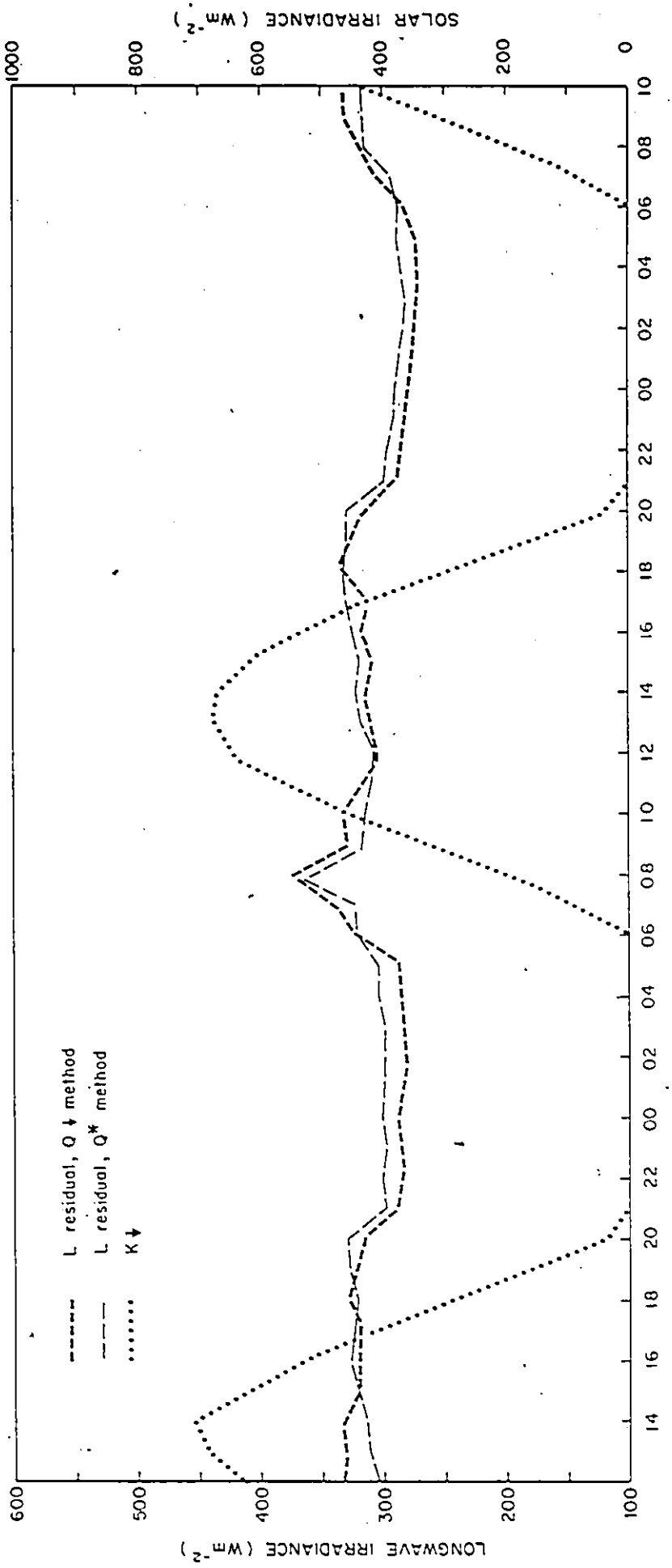

Figure 7: Comparison of the Q* and Q↓ methods of longwave irradiance at Churchill, Manitoba. August 23-25, 1978. (Q* values courtesy of W.R. Rouse).

CHAPTER V

MODEL ESTIMATES OF LONGWAVE IRRADIANCE

A. Flux Emissivity

Results of the flux emissivity models are compared with measured irradiance L_{SIL} in Figures 8 and 9 for 1200Z, corresponding to the time of the morning radiosonde release at Buffalo. Similar comparisons are shown in Figures 10 and 11 for the 2300Z ascents. These data points represent a range of atmospheric conditions. All values are tabulated in Appendix B. The data show that both ELDOWN and SANDJ always agree to within 11%. Differences may be related to the use of temperature-dependent emissivities in SANDJ. Figure 12 shows the H_2O emissivities used in the models. For all pathlengths, the Staley and Jurica (1970) emissivities exceed those of Kuhn (1963). This may partly explain why SANDJ estimates always exceed those of ELDOWN.

Figures 8-11 indicate good agreement between model and measured irradiances. Both models however, usually under-estimate L_{SIL} at 1200Z as shown in Figures 8 and 9. ELDOWN under-estimates L_{SIL} for 15 of the 18 ascents by up to 16%, while SANDJ underestimates L_{SIL} for 12 of the 18 ascents by up to 5%. For the remaining ascents, two fluxes are over-estimated by up to 6% (ELDOWN) and three are over-estimated by up to 15% (SANDJ). For the 2300Z calculations, Figures 10 and 11 indicate

Figure 8: Comparison of calculated (ELDOWN) and measured irradiance L_{SIL} for 1200Z.

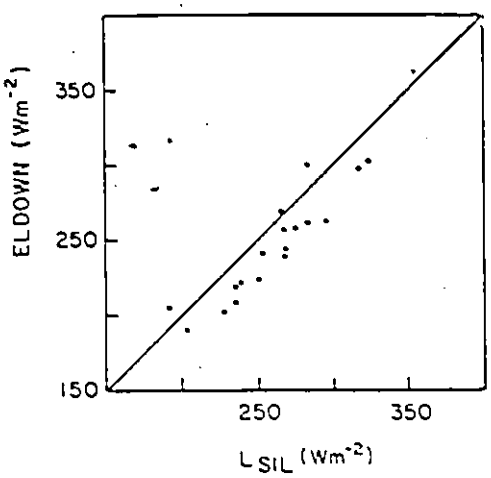

Figure 9: Comparison of calculated (SANDJ) and measured irradiance L_{SIL} for 1200Z.

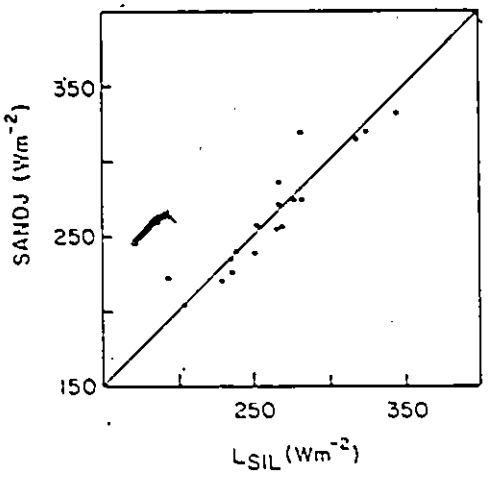

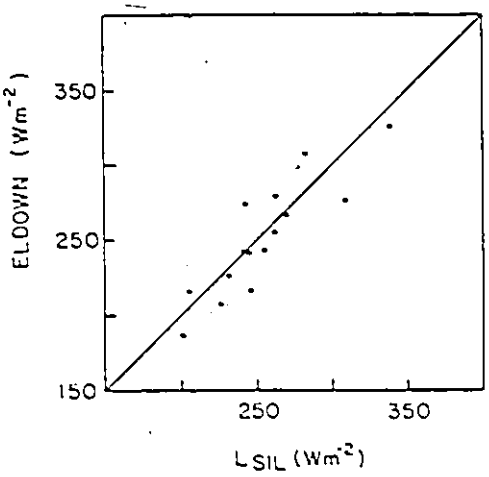

Figure 10: Comparison of calculated (ELDOWN) and measured irradiance L_{SIL} for 2300Z.

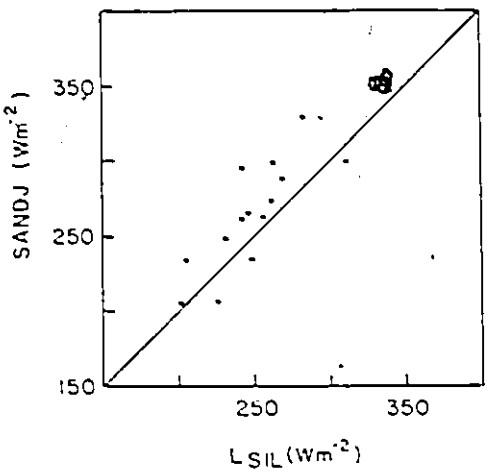

Figure 11: Comparison of calculated (SANDJ) and measured irradiance L_{SIL} for 2300Z.

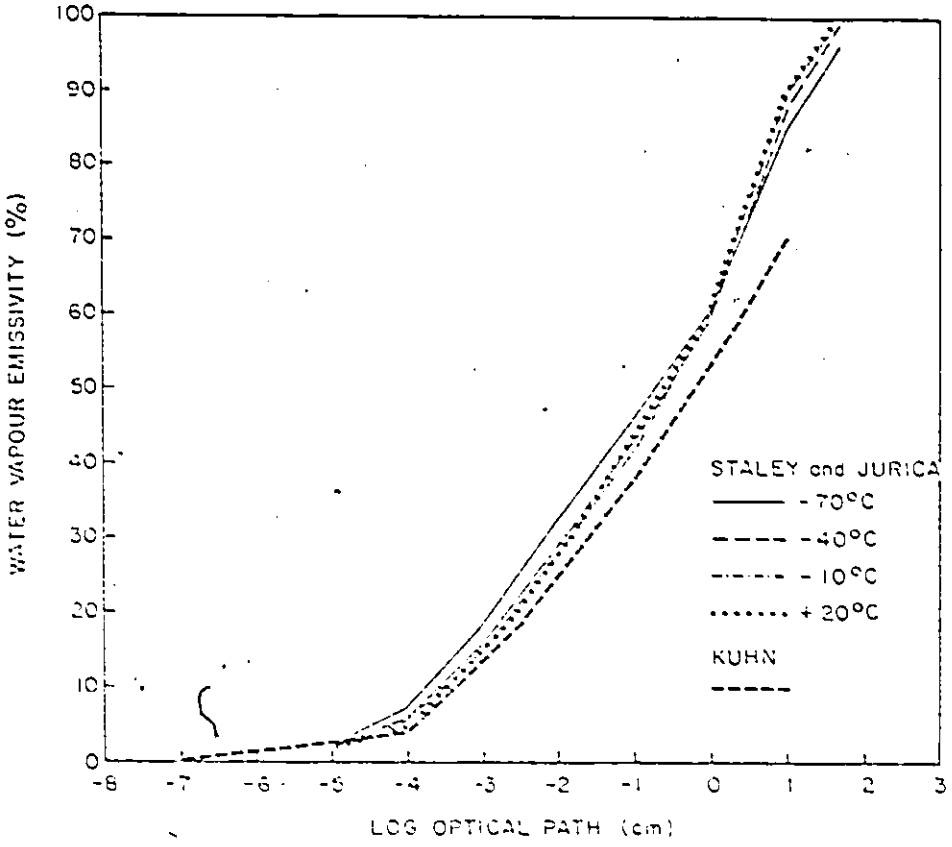

Figure 12: Water vapour emissivities of Staley and Jurica (1970) and Kuhn (1963).

good agreement between both FEM estimates and L_{SIL}, but the frequency of SANDJ model over-estimation increases. Data show that SANDJ over-estimates L_{SIL} for 12 of 15 ascents by up to 21% while ELDOWN over-estimates L_{SIL} for only 3 of the ascents by up to 12%.

Differences between measured and calculated irradiances may be considered from three points of view. Firstly, measured irradiances were obtained from the real atmosphere which contains other gases and contaminants which are often unknown, and are not included in the models. Model estimates are based on an input of pressure, temperature and amounts of H_2O and CO_2 only. It is hypothesized that no single minor atmospheric constituent (as already shown for O_3, CH_4 and N_2O) is highly significant, but that the total contribution of emissions from these and other gases may explain some of the difference between measured and calculated irradiances. Secondly, the use of a Buffalo temperature profile for the Hamilton atmosphere may not be appropriate. In principle, differences must exist in the temperature structure of these two atmospheres, especially in the planetary boundary layer. SANDJ, with its temperature-dependent emissivities may be more sensitive to such differences. Thirdly, it must be realized that although the measured irradiances L_{SIL} are thought to be the most reasonable measured values obtained from the intercomparison of instrumental determinations, these data are still dependent on the accuracy of the sensor used.

B. Empirical

The three empirical models were evaluated for five days. Results for air temperatures above and below freezing will be discussed separately and are presented in Tables 1 and 2.

(i) $T > 0^{o}C$

Of the two temperature-based models, estimates using the Idso-Jackson model were found to agree to within 11% of measured irradiances. The Swinbank model, in its original form (Equation 24) sometimes under-estimated hourly measured values by up to 13% and on other occasions over-estimated by up to 5%. These estimates have been modified to include two corrections suggested by Paltridge (1970): $+6Wm^{-2}$/tenth of cloud and a daytime correction ranging from $+15Wm^{-2}$ to $-30Wm^{-2}$ depending on time of day and season. This latter correction is to account for the apparent bias toward inversion conditions in the Swinbank model. With these corrections the Swinbank model sometimes under-estimated L_{SIL} by up to 13% and on other occasions over-estimated by up to 9%. Paltridge (1970) has suggested that the Swinbank model over-estimates in early afternoon. This trend is only apparent for April 18, using equation 24. Arnfield (1979) suggests that the Idso-Jackson model over-estimates in late afternoon and evening and under-estimates at all other times. The calculations in Table 1 show that the model may

TABLE 1: PERFORMANCE OF THE SWINBANK (L_{SWIN}), IDSO-JACKSON (L_{IJ}) AND BRUNT (L_B) EMPIRICAL MODELS FOR ESTIMATING LONGWAVE IRRADIANCE FOR AIR TEMPERATURE (T) > 0°C.

DAY	TIME	CLOUD (tenths)	T	L_{SIL}	$L_{SWIN(1)}$	DIFF(%)	$L_{SWIN(2)}$	DIFF(%)	L_{IJ}	DIFF(%)	L_B	DIFF(%)
Mar. 16	1600	0	1.7	248	228	-8	228	-8	239	-4	246	-1
	1700	0	1.9	253	229	-9	229	-9	240	-5	245	-3
	1800	0	0.6	253	229	-9	229	-9	235	-7	238	-6
Mar. 17	0800	0	0.2	253	221	-13	236	-7	233	-8	236	-7
	0900	2	2.1	264	230	-13	257	-3	240	-9	242	-8
	1000	0	3.2	267	236	-12	251	-6	245	-8	245	-8
	1100	0	5.5	286	248	-13	256	-10	254	-11	252	-12
	1200	0	7.1	292	256	-12	256	-12	261	-11	258	-12
	1300	0	8.4	300	264	-12	261	-13	268	-11	262	-13
	1400	1	10.0	304	273	-10	273	-10	276	-9	267	-12
	1500	1	10.2	300	274	-9	274	-9	277	-8	269	-10
	1600	2	11.0	267	279	+4	291	+9	281	+5	271	+1
	1700	3	10.0	267	273	+2	296	+11	276	+3	268	0
Apr. 18	0600	1	1.8	233	229	-2	235	+1	239	+3	241	+3
	0700	1	3.4	239	237	-1	246	+3	245	+3	247	+3
	0800	1	5.8	253	249	-2	255	+1	256	+1	255	+1
	0900	0	7.3	256	258	+1	255	0	262	+2	262	+2
	1000	0	9.0	268	267	0	256	-4	271	+1	267	0
	1100	0	10.0	273	273	0	255	-7	276	+1	271	-1
	1200	1	10.8	286	277	-3	260	-9	280	-2	273	-5
	1300	1	12.1	286	285	0	263	-8	287	0	279	-2
	1400	1	12.1	281	285	+1	262	-7	287	+2	279	-1
	1500	1	12.5	280	288	+3	264	-6	290	+4	285	+2
	1600	1	12.1	280	285	+2	263	-6	287	+3	283	+1
	1700	0	12.4	279	287	+3	262	-6	289	+4	283	+1
	1800	0	10.9	266	278	+5	263	-1	281	+6	275	+3

DAY	TIME	CLOUD	T	L_{SIL}	$L_{SWIN(1)}$	DIFF(%)	SWIN(2)	DIFF(%)	L_{IJ}	DIFF(%)	L_B	DIFF(%)
Apr. 19	1900	1	9.2	258	269	+4	270	+5	272	+5	271	+5
	2000	1	7.9	250	261	+4	267	+7	265	+6	264	+6
	2100	1	7.2	247	257	+4	268	+9	262	+6	262	+6
June 25	1200	0	18.0	345	322	-7	299	-13	324	-6	299	-13
	1300	1	18.9	344	328	-5	306	-11	330	-4	301	-13
	1400	1	20.2	349	337	-3	314	-10	339	-3	308	-12
	1500	1	19.8	345	335	-3	336	-3	337	-2	308	-11
	1600	1	19.7	338	334	-1	312	-8	336	-1	306	-9
	1700	0	20.0	337	336	0	311	-8	338	0	305	-9
	1800	0	19.6	337	333	-1	318	-6	335	-1	303	-10
	1900	0	18.5	330	326	-1	321	-3	328	-1	297	-10
	2000	1	15.3	327	305	-7	311	-5	307	-6	283	-13

*DIFF = % DIFFERENCE BETWEEN MEASURED IRRADIANCE L_{SIL} AND THE MODEL ESTIMATE. + INDICATES MODEL OVER-ESTIMATION, - INDICATES MODEL UNDER-ESTIMATION

**$L_{SWIN(1)}$ CALCULATED USING EQUATION (24), $L_{SWIN}(2)$ CORRECTED FOR CLOUD AND TIME OF DAY.

either over- or under-estimate. Differences between published results and those calculated here may be explained in part by instrumental differences and the fact that these models may not be generally applicable to different geographic sites since all are regression-based. Arnfield (1979) has also noted that his results are different in trend from those of Paltridge (1970) and Idso (1972). The Brunt and Idso-Jackson model results are similar. Swinbank's model however, shows the best agreement with measured irradiance for $T > 0^{o}C$.

(ii) $T < 0^{o}C$

Idso (1972) has shown that the Swinbank model performs poorly when air temperatures are below freezing. Calculations for Hamilton show that the original Swinbank formula ($L_{SWIN(1)}$) always under-estimates measured irradiance by 4-15%. There is some hint in the data for March 17 (Table 1) that as air temperatures become warmer, model estimates improve. When cloud and daytime corrections are applied to the Swinbank model (Table 2) values sometimes under-estimate L_{SIL} by up to 13% and on other occasions over-estimate by up to 6% for air temperatures below freezing. The Idso-Jackson model under-estimates by up to 9% for small negative temperatures (-0.1 - $-1.4^{o}C$). The Brunt equation severely over-estimates by up to 40% at large negative temperatures. At small negative temperatures, the Brunt equation under-estimates by up to 7%.

TABLE 2: PERFORMANCE OF THE SWINBANK (L'_{SWIN}), IDSO-JACKSON (L_{IJ}) AND BRUNT (L_B) EMPIRICAL MODELS FOR ESTIMATING LONGWAVE IRRADIANCE FOR AIR TEMPERATURE (T) < 0°C.

DAY	TIME	CLOUD	T	L_{SIL}	$L_{SWIN(1)}$	DIFF(%)	$L_{SWIN(2)}$	DIFF(%)	L_{IJ}	DIFF(%)	L_B	DIFF(%)
Feb. 11	1300	1	-15.9	168	153	-9	153	-9	195	+16	233	+39
	1400	1	-16.9	166	150	-10	150	-10	193	+16	226	+36
	1500	1	-16.0	162	153	-6	153	-6	194	+20	226	+40
	1600	1	-16.7	162	151	-7	157	-3	193	+19	223	+38
	1700	2	-16.7	158	151	-4	168	+6	193	+22	221	+40
	1800	2	-17.9	160	146	-9	165	+3	191	+19	217	+36
	1900	1	-19.1	162	142	-12	161	-1	189	+17	215	+33
Mar. 16	1900	0	-0.1	246	219	-11	232	-6	232	-6	237	-4
	2000	0	-0.2	246	219	-11	232	-6	232	-6	237	-4
	2100	0	-0.3	246	218	-11	231	-6	232	-6	237	-4
Mar. 17	0600	0	-1.1	246	215	-13	215	-13	229	-7	234	-5
	0700	0	-1.4	251	213	-15	228	-9	228	-9	233	-7

*DIFF = % DIFFERENCE BETWEEN MEASURED IRRADIANCE L_{SIL} AND THE MODEL ESTIMATE. + INDICATES MODEL OVER-ESTIMATION, - INDICATES MODEL UNDER-ESTIMATION.

**$L_{SWIN(1)}$ CALCULATED USING EQUATION (24), $L_{SWIN(2)}$ CORRECTED FOR CLOUD AND TIME OF DAY.

CHAPTER VI

THE ROLE OF AEROSOL IN THE INFRARED

A. Case Studies

It is usually assumed that tropospheric aerosols significantly affect solar irradiance but have little effect on longwave irradiance (Mitchell, 1971; Yamamoto and Tanaka, 1972; Chýlek and Coakley, 1974). From Mie theory, values of extinction efficiency, and therefore of optical depths, in the infrared (eg. wavelength of 10 μm) are at least one order of magnitude smaller than those for visible wavelengths (0.5 μm). This is shown in the inset to Figure (13). However, Coakley and Grams (1976) point out that aerosol may have a larger effect in the infrared than at solar wavelengths if the aerosol is composed of extremely small particles ($x < < 1$). Figure 13 summarizes their findings where Q_{ext} increases over the range of small absorbing particles ($.001 < x < 1.0$) as n_{IM} varies between 0.001 and 0.5. For $x > > 1$ the effects in the infrared are thought to be small because there are few particles in this size range due to fallout. For $x < < 1$, Q_{abs} may exceed Q_{sca} when $n_{IM} > 0$ and for particles which absorb, Q_{ext} in the infrared may be larger than Q_{ext} at visible wavelengths. In an experimental study, however, Rouse and McCutcheon (1970) showed opposing evidence

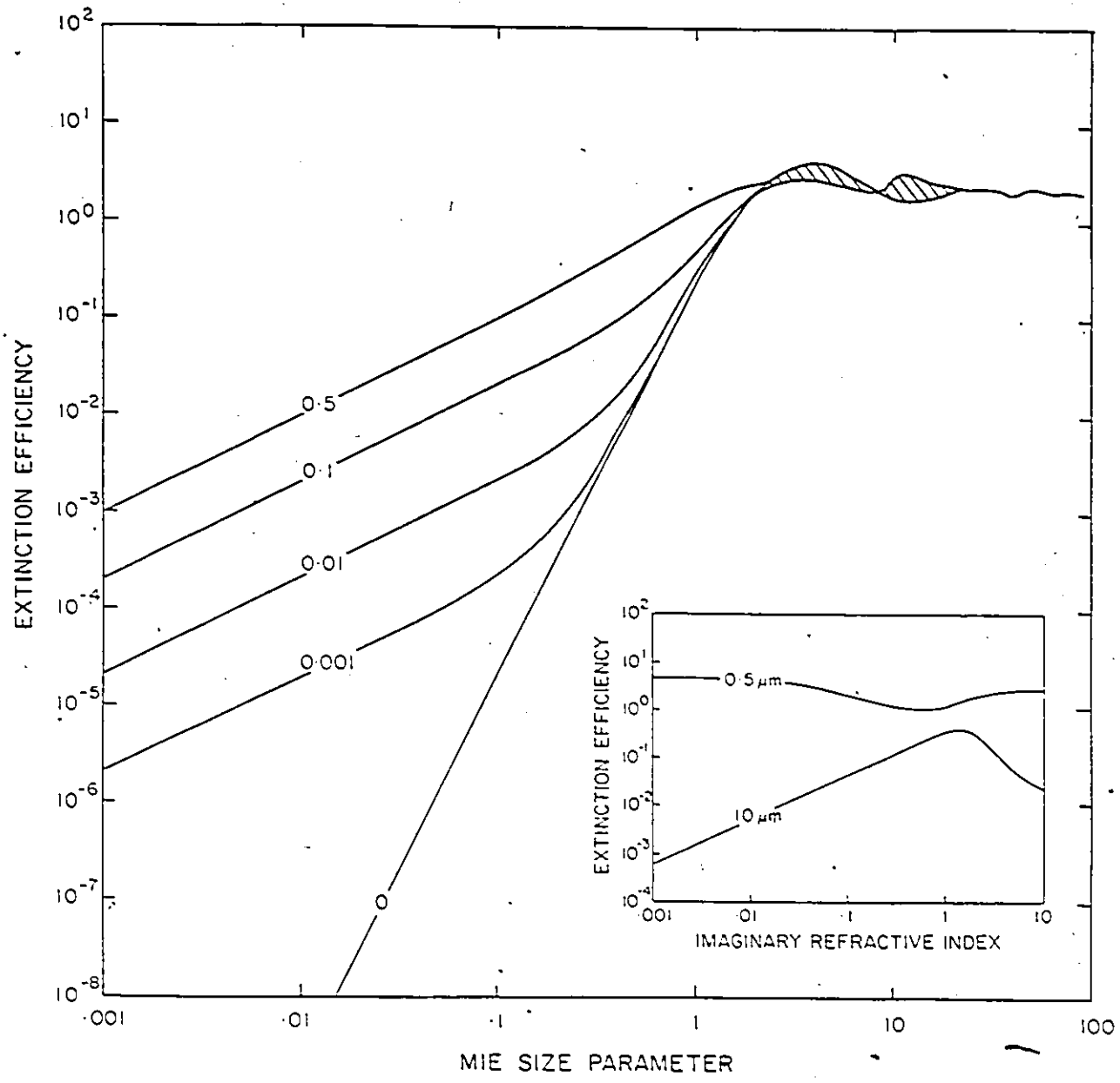

Figure 13: Extinction efficiency factor as a function of the Mie size parameter and the imaginary refractive index. The real part of the index of refraction is taken to be 1.5. Curves in the inset are for a spherical particle having a radius of 0.3 μm.

that at Hamilton, Ontario, there was an 11% increase in measured longwave irradiance at an industrial site when compared to a control site on the western edge of the city at McMaster University.

B. Aerosol effects at peak solar and infrared wavelengths

To quantify the role of aerosol at solar and infrared wavelengths, values of absorption (1 - w) and backscatter wß at λ=0.5 μm and λ=10.0 μm were computed. These values were derived for radii between < 1 μm and 10 μm using graphs published by Kellogg et al. (1979) which show (Figure 14) the variation of (1 - w) and wß with particle radius and n_{IM} for λ=0.5 μm. The real part of the refractive index is 1.5. Values for other wavelengths can be obtained from the graphs by multiplying the radius values by 0.5 μm/λ. Results for λ=10.0 μm are shown in Figure 15 for n_{IM} = 0.01 and n_{IM} = 0.1, for $0.0 < r \leq 10$ μm. At solar wavelengths, absorption reaches a minimum at r=0.2 μm (log r = -0.7) for n_{IM} = 0.01 and 0.1, then increases gradually and becomes constant over the range 4 - 10 μm (log r = 0.6 - 1.0) for both values of n_{IM}. In the infrared, maximum absorption occurs at $r \leq 0.02$ μm (log r = -1.7) for n=0.01 and at $r \leq 0.05$ μm (log r = -1.3) for n = 0.1, then decreases rapidly in both cases reaching a minimum at r = 0.2 μm (log r = -0.7) then increasing only slightly up to r = 0.5 μm (log r = -0.3).

Figure 16 is also derived from the graphs of Kellogg et al. (1979). In this plot, values of absorption and backscatter are shown as a function of n_{IM} for a particle of modal radius r_c = 0.7 μm assuming a

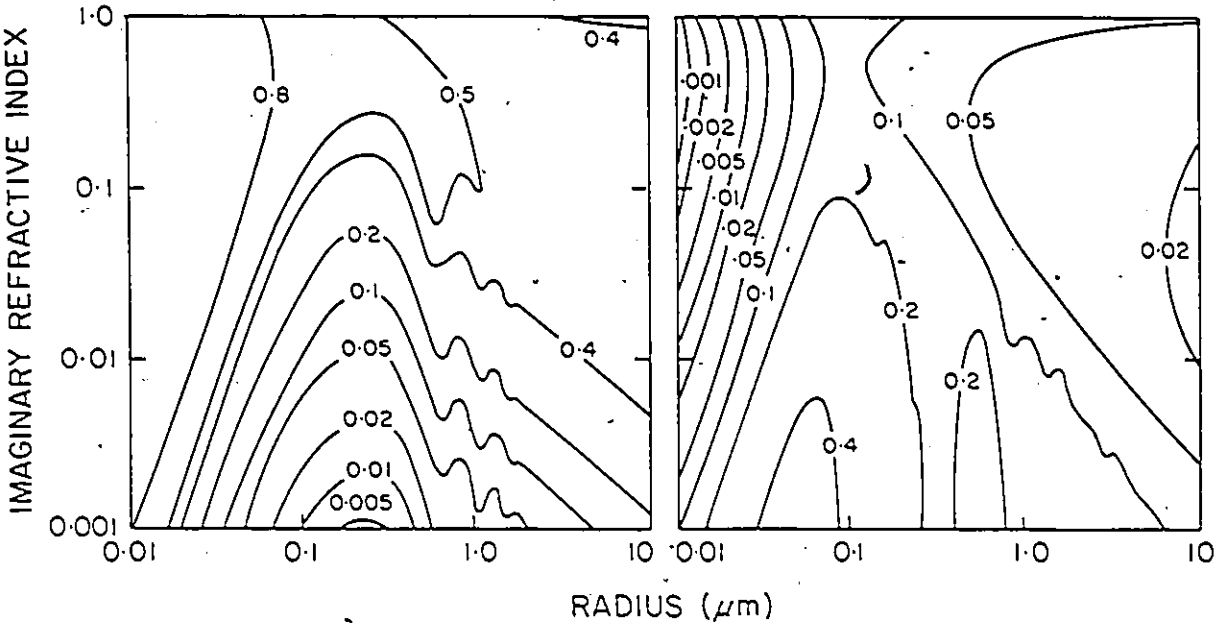

Figure 14: Optical properties of spherical particles at a wavelength λ=0.5 μm The real part of the refractive index is taken to be 1.5. The curves show isopleths of absorption (1 - w) on the left and backscatter $w\beta$ on the right. Results for other wavelengths may be obtained from these graphs by multiplying the values of the radius by 0.5 μm/λ (Kellogg et. al., 1979).

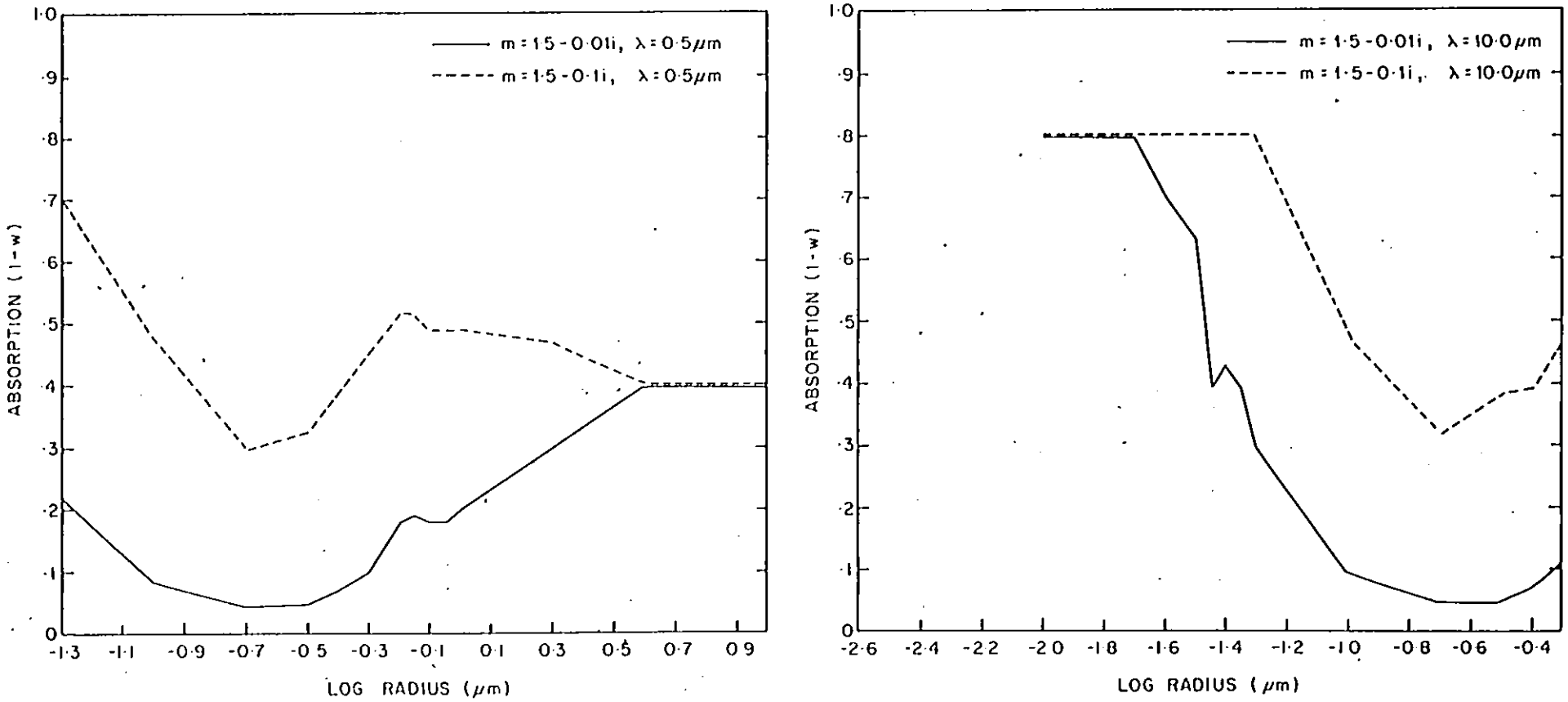

Figure 15: Absorption for different values of the imaginary part of the refractive index at λ=0.5 μm (left) and λ=10.0 μm (right). Values are derived from Figure 14.

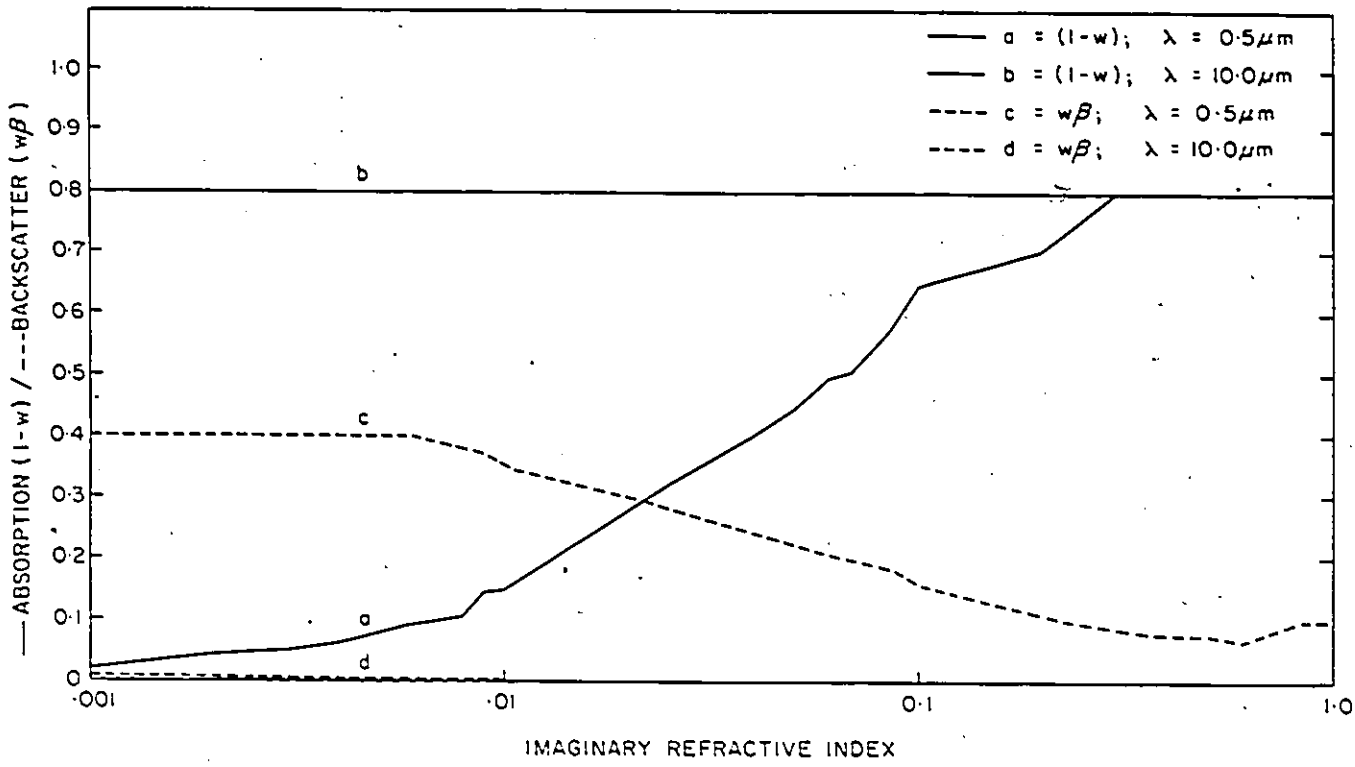

Figure 16: Absorption (1 - w) and backscatter wβ for a particle of modal radius r=0.07 μm (assuming a Haze L distribution) and an imaginary index with the real part set equal to 1.5 and the imaginary part varying between 0.001 and 1.0 for peak solar at 0.5 μm and peak infrared at 10 μm. Values of (1 - w) and wβ were derived following Kellogg et. al. (1979).

Haze-L distribution for continental aerosol (Diermendjian, 1969). The real part of the refractive index is 1.5 and n_{IM} varies from 0.001 to 1.0. The variation of (1 - w) and wß are shown for λ=0.5 μm (peak solar) and for λ=10.0 μm (peak infrared). Differences for various values of n_{IM} are tabulated in Table 3.

Values of wß in the infrared were obtained by linear extrapolation of all curves in the original Kellogg et. al (1979) plot. In the case of (1 - w), a value of 0.8 was assumed for all values of n_{IM}. The graph shows that at peak infrared, (1 - w) is therefore, constant at 0.8 while the backscatter may be assumed zero at all values of n_{IM}. At peak solar, both parameters vary widely, with wß reaching a maximum at n_{IM}=0.001 and decreasing as n_{IM} increases, over the range of n_{IM} plotted. At n_{IM}>0.3, absorption at peak infrared equals absorption at peak solar. At all values of n_{IM}<0.3 absorption is always significantly greater in the infrared. Coakley and Grams (1976) have shown that Q_{ext} is almost constant as n_{IM} ranges between 0.001 and 10.0 at λ=0.5 μm, but varies widely at λ=10 μm, with minima at n_{IM}=0.001 and 10.0 and a maximum at about n_{IM}=1.0 (Figure 13). At all values of n_{IM} however, Q_{ext} at 0.5 μm exceeds that at 10 μm by at least one order of magnitude. If Q_{ext} is smaller at infrared wavelengths, then the optical depth for aerosol at infrared wavelengths will also be small (Equation 10).

TABLE 3: Absorption (1 - w) and backscatter wß values for different values of n_{IM} for peak solar and infrared wavelengths.

r_c(μm)*	n_{RE}	n_{IM}	λ=0.5 μm (1 - w)	λ=0.5 μm wß	λ=10.0 μm (1 - w)	λ=10.0 μm wß
0.07	1.5	0.001	0.02	0.40	0.8	0.005
		0.01	0.15	0.35	0.8	0.001
		0.1	0.65	0.16	0.8	0.001
		1.0	0.79	0.10	0.8	0.001

*note in the scale conversion, r_c=0.0035 for λ=10 μm.

**w=single scattering albedo.

C. Model calculations

The findings of Kellogg et al., (1979) and Coakley and Grams (1976) suggest that aerosol may have some effect in the infrared, but uncertainty surrounds its evaluation. This uncertainty is apparent from calculations made in this study. Using the Q↓ method, Rouse and McCutcheon (1970) and Rouse et al., (1973) measured longwave irradiance at a Hamilton industrial site and at McMaster. Rouse and McCutcheon (1970) reported irradiances that are 11% higher on average at the industrial site than at McMaster. Table 4 summarizes the findings of Rouse et al., (1973). At night, ratios of longwave irradiance at the two sites are virtually unity. During the day however, when pyrradiometer measurements are influenced by solar heating, these ratios increase dramatically. Rouse and McCutcheon (1970) and Rouse et al., (1973) attribute the enhancement of irradiance at the industrial site to pollutants. The possible effect of aerosol is investigated here.

From Mie theory, values of the extinction coefficient β have been calculated (Table 5a) for several n_{IM} values for model atmospheres with "clear" (23km visibility) and "hazy" (5km visibility) aerosol concentrations as defined by McClatchey et al., (1972). Values of n_{IM} deduced experimentally by Pueschel and Kuhn (1975) for urban and rural aerosol at Phoenix, Arizona are also included. Table 5a shows that even for heavily absorbing particles (n_{IM}=1.0) β reaches a

maximum of only 0.86×10^{-2}. Table 5b shows calculated fluxes from RADVERS using a range of β values between 0.0001 and 1.0. These calculations indicate that a β value of 0.5 is required to obtain an 11% increase in measured irradiance found by Rouse and McCutcheon (1970). All values in Table 5a are at least an order or magnitude smaller than the required range. In fact, if $\beta = 0.86 \times 10^{-2}$, the percentage increases in model irradiance are only 0.23, 0.29 and 0.58% for February 20, March 23 and August 21, respectively. Hence, the increase in irradiance reported by Rouse and McCutcheon (1970) is unlikely to be due to aerosol. It is more likely to be due to instrumental error of the daytime longwave flux or to a daytime increase in radiation emission from trace gases.

Gaseous effects have not been investigated in this study. However, some inferences can be drawn. Since the atmosphere is black at all wavelengths, except those within the atmospheric window, pollutant gases can only influence irradiance within the 8 - 13 μm waveband. This band contains approximately 30% of the irradiance. To a first approximation (Paltridge, 1970) the contribution of a pollutant gas can be defined as

$$\Delta L = 0.3\, \varepsilon_g \sigma \bar{T}^4 \qquad (29)$$

where ε_g is the emissivity of the layer in which the gas occurs and

$\bar{T}$ is the average temperature of that layer. The transmission spectra for N_2O, CH_4, NH_3, HNO_3, C_2H_4 and SO_2 (Wang et al., 1976) indicate that values of ε_g are much less than 0.05. Using surface (base of the radiosonde) temperatures for February 20, March 23 and August 21, ΔL has values between 4 and 5 Wm^{-2}. Higher temperatures have negligible effects. If T is increased by $30^{o}K$ the maximum value of ΔL is only 8 Wm^{-2}. Hence, large differences (~ 10%) in irradiance between residential and industrial locations are difficult to justify. The tentative estimates of the effects of aerosol and trace gases on irradiance clearly do not account for the enhanced values of irradiance reported by Rouse and McCutcheon (1970) and Rouse et. al., (1973). Table 4 and Appendix B show that the measured irradiance values reported by Rouse et al., (1973) for the residential site are of similar magnitude to the 1979 measurements in March. However, the Rouse et al., (1973) values of irradiance in March for the industrial zone are of comparable magnitude to values obtained in the warmer months of 1979. It is not clear how this can be the case.

Table 4: Hourly values of longwave irradiance (Wm^{-2}) at an industrial L_{IND} and a residential L_E site at Hamilton and ratios of the two irradiances for March 27, 1972. (Rouse et. al., 1973).

Hour	L_{IND}	L_{RE}	L_{IND}/L_{RE}
01	181	188	0.96
02	171	184	0.93
03	164	174	0.94
04	166	171	0.97
05	170	172	0.99
06	192	189	1.02
07	205	179	1.15
08	253	182	1.39
09	303	187	1.62
10	318	196	1.62
11	279	202	1.38
12	259	204	1.27
13	339	206	1.64
14	326	210	1.55
15	345	204	1.69
16	314	208	1.51
17	280	211	1.32
18	239	207	1.13
19	207	203	1.02
20	186	186	1.00
21	192	190	1.01
22	189	187	1.01
23	196	194	1.01
24	196	192	1.02

Table 5: (a) β values from Mie theory

N_{RE}	N_{IM}	β(23 km)	β(5 km)
1.5	0.001	$.45 \times 10^{-3}$	$.23 \times 10^{-2}$
1.5	0.01	$.45 \times 10^{-3}$	$.22 \times 10^{-2}$
1.5	0.08*	$.44 \times 10^{-3}$	$.22 \times 10^{-2}$
1.5	0.1	$.44 \times 10^{-3}$	$.22 \times 10^{-2}$
1.5	0.5**	$.74 \times 10^{-3}$	$.37 \times 10^{-2}$
1.5	1.0	$.17 \times 10^{-2}$	$.86 \times 10^{-2}$

* Pueschel and Kuhn (1975), rural aerosol
** Pueschel and Kuhn (1975), urban aerosol

(b) RADVERS calculated irradiances (Wm^{-2}) corrected for aerosol+

β	FEB. 20	(%)	MAR. 23	(%)	AUG. 21	(%)
0.0001	189.71	0.0	257.19	0.0	296.88	0.0
0.001	189.76	0.03	257.27	0.03	297.07	0.07
0.009	190.14	0.23	257.94	0.29	298.60	0.58
0.01	190.21	0.26	258.06	0.34	298.88	0.68
0.05	192.10	1.3	261.43	1.7	306.43	3.2
0.1	194.21	2.4	265.33	3.2	314.77	6.0
0.5	203.88	7.5	287.07	11.6	354.08	19.3
1.0	206.10	8.6	300.44	16.8	373.50	25.8

%=PERCENTAGE INCREASE FROM CALCULATED FLUX WITHOUT AEROSOL.

\+ aerosol layer defined as 2 km thick, between surface and pressure of 79.5 kPa (U.S. Standard Atmosphere).

CHAPTER VII

CONCLUSIONS

Measurements of longwave irradiance at the ground were made under cloudless or near cloudless skies. Three instrumental determinations were used and results showed that the silicon-domed Eppley pyrgeometer provided the most reasonable daytime measurements of longwave irradiance. The earlier Eppley pyrgeometer model equipped with a KRS-5 dome was shown to over-estimate during the day while it provided satisfactory nocturnal measurements. Using the residual method, pyrradiometers provided acceptable estimates of irradiance at night. Increased irradiance near sunrise and sunset and a mid-day minimum may be a feature of the particular sensor used although the latter is evident in GATE data. The placing of the blackbody cavity in a styrofoam block had minimal effect on reducing cavity temperature.

Using the flux emissivity approach, calculations were performed using Buffalo radiosonde data, the closest station to the measurement site with balloon ascents. It is difficult to assess the errors which might occur in applying these profile data to the Hamilton atmosphere. There may be significant boundary layer differences between the two sites, but at higher levels, these differences should be minimal. The flux emissivity model estimates were found to agree well with measured

irradiance over a wide range of atmospheric temperatures. There was a tendency for SANDJ; the model employing the temperature-dependent emissivities of Staley and Jurica (1970), to over-estimate measured irradiance for the 2300Z ascents. Results from empirical formulae agree with measured values to within ± 13% for air temperatures above freezing. For temperatures below freezing, the Swinbank equation usually under-estimates measured irradiance. At large negative temperatures, the Idso-Jackson and Brunt models performed very poorly.

The effect of aerosol was difficult to determine. Theory suggests that aerosols have little effect in the infrared because of their small optical depths (Paltridge and Platt, 1976). Coakley and Grams (1976) have shown that this may not be the case if the aerosol layer is composed of very small particles ($x \ll 1$) which absorb strongly at infrared wavelengths. Aerosol effects could not be determined without knowledge of the size, number distributions and optical properties. Estimates from Mie theory calculations showed that the large difference in irradiance between the industrial and residential sites in Hamilton, reported by Rouse and McCutcheon (1970) and Rouse et al., (1973), are too large to be due to aerosols.

Although this study has provided new evidence on the measurement of longwave irradiance and has tested various empirical and physical approaches to evaluating flux densities, there is need for future research

in this area of radiative transfer. A network of pyrgeometers mounted at sites in a rural area adjacent to an industrial-urban area would be useful in determining both spatial differences in longwave radiation and in the relative contribution of urban pollutants when compared to a relatively clean rural atmosphere. On-site radiosonde or tethersonde profiles would also be useful, so that site-specific pressure, temperature, and humidity data could be used in model calculations.

REFERENCES

Ackerman, T.P., Liou, K.N. and C.B. Leovy, 1976. Infrared radiative transfer in polluted atmospheres. J. Appl. Meteorol., 15, 28-35.

Albrecht, B. and S.K., Cox, 1977. Procedures for improving pyrgeometer performance. J. Appl. Meteorol., 16, 188-197.

Arnfield, A.J. 1979. Evaluation of empirical expressions for the estimation of hourly and daily totals of atmospheric long-wave emission under all sky conditions. Quart. J. Royal Meteorol. Soc., 105, 1041-1052.

Brunt, D., 1932. Notes on radiation in the atmosphere. Quart. J. Roy. Meteorol. Soc., 58(247), 389-420.

Chýlek, P. and J.A. Coakley, 1974, Aerosols and Climate. Science, 183, 75-77.

Coakley, J.A. and G.W. Grams, 1976. Relative influence of visible and infrared optical properties of a stratospheric aerosol layer on the global climate. J. Appl. Meteorol., 15, 679-691.

Davies, J.A. and W. Schertzer, 1974. Canadian radiation measurements and surface radiation balance estimates for Lake Ontario during IFYGL. Final Report, Government of Canada, Dept. of the Environment, Canada Centre for Inland Waters, Great Lakes Division, Burlington, Ontario. 77p.

Davies, J.A. and T.C. Uboegbulam, 1978. Parameterization of surface incoming radiation in tropical cloudy conditions. Atmosphere-Ocean, 17(1), 14-23.

Deacon, E.L., 1970. The derivation of Swinbank's long-wave radiation formula. Quart. J. Roy. Meteorol. Soc., 96, 313-319.

Deirmendjian, D., 1969. Electromagnetic Scattering on Spherical Polydispersions. Elsevier, New York, 290 p.

Enz, J.W., Klink, J.C. and D.G. Baker, 1975. Solar radiation effects on pyrgeometer performance. J. Appl. Meteorol., 14, 1297-1302.

Idso, S.B., 1972. Systematic deviations of clear sky atmospheric thermal radiation from predictions of empirical formulae. Quart. J. Roy. Meteorol. Soc., 98, 399-401.

Idso, S.B., 1974. On the use of equations to estimate atmospheric thermal radiation. Arch. Met. Geoph. Biokl. Ser. B. 22(e), 287-299.

Idso, S.B. and R.D. Jackson, 1969. Thermal radiation from the atmosphere J. Geophys. Res., 74(23), 5397-5403.

Kellogg, W.W., J.A. Coakley and G.W. Grams, 1979. Proc. WMO/IAMAP Symp. on long term climatic fluctuations, Norwich, U.K. W.M.O. DOL 421, Geneva, 323-330.

Kuhn, P.M., 1963. Radiometersonde observations of infrared flux emissivity of water vapour. J. Appl. Meteorol. 2(2), 268-378.

Kuhn, P.M., Weickmann, H.K., Lojko, M.J. and L.P. Stearns, 1974. Transfer of infrared radiation through clouds. Appl. Optics, 13(3), 512-517.

Kuhn, P.M., 1976. RADVERS (CDC 6400 Version), Atmospheric Physics and Chemistry Laboratory, NOAA, Boulder, Colorado, U.S.A.

McClatchey, R.A., R.W. Fenn, J.E.A. Selby, F.E. Volz and J.S. Garing, 1972. Optical properties of the atmosphere. Third edition Optical Physics Laboratory, Project 7670, Air Force Cambridge Research Laboratories, Bedford 108 p.

Mitchell, J.M., 1971. The effect of atmospheric aerosols on climate with special reference to temperature near the Earth's surface. J. Appl. Meteorol., 10, 703-714.

Monteith, J.L., 1964. Long-wave radiation from clear skies. Discussion, Quart. J. Roy. Meteorol. Soc., 90, 488-493.

Monteith, J.L., 1973. Principles of Environmental Physics, Arnold, London, 241 p.

Paltridge, G.W., 1970. Daytime long-wave radiation from the sky. Quart. J. Roy. Meteorol. Soc., 96(410), 645-653.

Paltridge, G.W. and C.M.R. Platt, 1976. Radiative processes in meteorology and climatology. Development in Atmospheric Science, 5, Elsevier, New York, 318p.

Polavarapu, R.J. 1978. Measurement of net radiation from shipboard sensors. J. Appl. Meteorol., 17, 1062-1067.

Pueschel, R.F. and P.M. Kuhn, 1975. Infrared absorption of tropospheric aerosols: urban and rural aerosols of Phoenix, Arizona. J. Geophys. Res., 80(21), 2960-2962.

Ramanathan, V., 1976. Radiative transfer within the earth's troposphere and stratosphere: a simplified radiative-convective model. J. Atmos. Sci., 33, 1330-1346.

Ramanathan, V. and Coakley, 1978. Climate modeling through radiative-convective models. Rev. Geophys. and Space Physics, 16(4), 465-489.

Robinson, P.J., J.A. Davies and M. Nunez, 1972. Longwave radiation exchanges over Lake Ontario. Fourth Report, March 1972. Government of Canada, Dept. of Environment, Canada Centre for Inland Waters, Great Lakes Division, Burlington, Ontario, 135 p.

Rodgers, C.D. and C.D. Walshaw, 1966. The computation of infra-red cooling rates in planetary atmospheres. Quart. J. Roy. Meteorol. Soc., 92, 67-92.

Rouse, W.R. and J.G. McCutcheon, 1970. The diurnal behaviour of incoming solar and infrared radiation in Hamilton, Canada. Climatologie, 191-196.

Rouse, W.R., D. Noad and J. McCutcheon, 1973. Radiation, temperature and atmospheric emissivities in a polluted urban atmosphere at Hamilton, Ontario. J. Appl. Meteorol., 12(5), 798-807.

Staley, D.O. and G.M. Jurica, 1970. Flux emissivity tables for water vapour, carbon dioxide and ozone. J. Appl. Meteorol., 9(3), 365-372.

Swinbank, W.C., 1963. Long-wave radiation from clear skies. Quart. J. Roy. Meteorol. Soc., 89(381), 339-348.

Uboegbulam, T.C., 1978. Estimation of the surface radiation balance and components for a tropical ocean. M.Sc. thesis, Dept. of Geography, McMaster University, Hamilton, Ontario. (unpublished).

Wang, W.C., Y.L. Yung, A.A. Lacis, T. Mo and J.E. Hansen, 1976. Greenhouse effects due to man-made perturbation of trace gases. Science, 194 (4266), 685-690.

Williamson, S.J., 1973. Fundamentals of Air Pollution, Addison-Wesley, Reading 472 p.

Yamamoto, G.Y. and M. Tanaka, 1972. Increase of global albedo due to air pollution. J. Atmos. Sci., 29, 8, 1405-1412.

APPENDIX A

DERIVATION AND SOLUTION OF THE RADIATIVE TRANSFER EQUATION FOR LONGWAVE RADIATION*

The change in intensity of a radiant beam travelling in direction r between two points P and P^1 which are a distance ds apart is given by

$$I_v(P^1, r) = I_v(P, r) + \frac{dI_v}{ds} ds \qquad (1)$$

where $I_v(P^1, r)$ and $I_v(P, r)$ are the spectral intensities at P and P^1 and v is wavenumber. In the general case of an absorbing, scattering and emitting medium the intensity changes are due to: attenuation by absorption expressed as

$$dI_v = -K_v I_v(P, r) \rho ds, \qquad (2)$$

where K_v is the mass absorption coefficient (kg^{-1}) and ρ is air density; attenuation by scattering, similarly expressed as

$$dI_v = -\sigma_v I_v(P, r) \rho ds, \qquad (3)$$

where σ_v is the mass scattering coefficient (kg^{-1}); and emission

*From unpublished notes by J.A. Davies.

$$dI_v = K_v I_{bv}(T) \rho ds, \tag{4}$$

where $I_{bv}(T)$ is the Planck function.

Intensity also increases by forward scattering of energy from rays emanating from all directions into direction r. A scattering function may be defined to specify the angular distribution of scattered radiation given by

$$\frac{1}{4\pi} p_v(P, r^1, r) \tag{5}$$

where r^1 is the direction of a second radiant beam. The contribution by scattering from all rays is obtained by integrating equation (5) over solid angle ω. Hence,

$$dI_v = \frac{\sigma_v}{4\pi} \int_{4\pi} I_v(P, r^1)\, p_v(P, r^1, r)\, d\omega^1 \rho ds \tag{6}$$

Equations (2), (3), (4) and (6) are the components of the radiative transfer equation for an absorbing, scattering and emitting medium. Summing these and dividing by $\cos\theta\, d\tau_v$, where $d\tau_v = \rho\beta_v dz$, and Θ is the angle of incidence, and β_v is the total extinction coefficient, $K_v + \sigma_v$,

$$\cos\theta \frac{dI_v}{d\tau_v} = - I_v(\tau_v, r) + \frac{\sigma_v}{\beta_v 4\pi} \int_{4\pi} I_v(\tau_v, r^1) p_v$$

$$(\tau_v, r^1, r)\, d\omega + \frac{k_v}{\beta_v} I_{bv}(\tau_v) \qquad (7)$$

For longwave radiation in a cloudless, aerosol-free atmosphere, the mass scattering coefficient is zero, and equation (7) reduces to

$$\mu \frac{dI_v}{d\tau_v} = I_{bv}(\tau_v) - I_v(\tau_v) \qquad (8)$$

where $\mu = \cos\theta$.

Re-arranging equation (8) and dividing through by μ this first order differential equation of the form

$$\frac{dI_v}{d\tau_v} + \frac{1}{\mu} I_v = \frac{I_{bv}}{\mu} \qquad (9)$$

is solved by multiplying through by the integrating factor $\exp\left(\int_0^{\tau} \frac{1}{\mu} d\tau\right)$ and integrating between the optical depth τ_o at an arbitrary reference level somewhere in the system and τ_1, the optical depth of the appropriate boundary of the system:

$$\int_{\tau_1}^{\tau_o} \frac{d}{d\tau} \left(e^{\tau/\mu} I_v\right) d\tau = \int_{\tau_1}^{\tau_o} e^{\tau'/\mu} \frac{I_{bv}}{\mu} d\tau' \qquad (10)$$

The intensity at τ_o may be expressed as

$$I_v(\tau_o) = e^{(\tau_1 - \tau_o)/\mu} I_v(\tau_1) + \int_{\tau_1}^{\tau_o} I_{bv} e^{(\tau_1 - \tau_o)} \frac{d\tau'}{\mu} \qquad (11)$$

Employing the boundary condition $I_v(\tau_1) = \varepsilon_s I_{bv}(\tau_1)$ where ε_s and I_{bv} are the emissivity and the blackbody radiant intensity of the boundary, equation (11) becomes

$$I_v(\tau_o) = \left[\varepsilon_s I_{bv}(\tau_1) e^{-(\tau_o - \tau_1)/\mu}\right] + \left[\int_{\tau_1}^{\tau_o} I_{bv} e^{-(\tau_o - \tau')/\mu} \frac{d\tau'}{\mu}\right] \qquad (12)$$

The first term on the right hand side of equation (12) accounts for the fraction of radiation emitted by the <u>boundary</u> which is transmitted to τ_o, while the second term represents the sum of contributions from the <u>layers</u> between the boundary and the reference level.

Flux density L at τ_o is obtained by multiplying intensity by μ and integrating over wavenumber and solid angle ω:

$$L(\tau_o) = \int_{\nu_1}^{\nu_2} d\nu \int_0^{2\pi} \varepsilon_s I_{b\nu}(\tau_1)\, \mu e^{-(\tau_o - \tau_1)/\mu}\, d\omega + \int_{\nu_1}^{\nu_2} d\nu \int_0^{2\pi} \int_{\tau_1}^{\tau_o} I_{b\nu}\, \mu e^{-(\tau_o - \tau^1)/\mu} \frac{d\tau^1}{\mu}\, d\omega \quad (13)$$

For simplicity, let the first term on the right hand side of equation (13) be L^1_ν and the second term by L^2_ν. Omitting the ν integration temporarily and substituting $d\omega = \sin\theta d\theta d\phi$, where ϕ is azimuth, L^2_ν becomes

$$L^2_\nu(\tau_o) = \int_{\tau_1}^{\tau_o} \int_0^{2\pi} \int_0^{\pi/2} I_{b\nu}\, e^{-(\tau_o - \tau^1)/\mu} \sin\theta d\theta d\phi d\tau^1 \quad (14)$$

Substituting $d\mu = -\sin\theta d\theta$,

$$L^2_\nu(\tau_o) = -\int_{\tau_1}^{\tau_o} \int_0^{2\pi} \int_1^0 I_{b\nu}\, e^{-(\tau_o - \tau^1)/\mu}\, d\mu d\theta d\tau^1 \quad (15)$$

and finally, substituting $d\mu = -dn/n^2$,

$$L^2_\nu(\tau_o) = \int_{\tau_1}^{\tau_o} \int_0^{2\pi} \int_1^\infty I_{b\nu}\, e^{-(\tau_o - \tau)n} \frac{dn}{n^2}\, d\theta d\tau^1 \quad (16)$$

Integrating over azimuth, assuming an isotropic source and using $B_\nu = \pi I_{b\nu}$, equation (16) becomes

$$2B_v \int_1^{\infty} e^{-(\tau_o - \tau^1)n} \frac{dn}{n^2} \tag{17}$$

which corresponds to the exponential integral of the form

$$E_{in}(x) = \int_1^{\infty} e^{-xn} \frac{dn}{n^n} \tag{18}$$

hence, equation (17) can be expressed as a second exponential integral where $n = 2$ and $x = (\tau_o - \tau^1)$:

$$E_{i2}(\tau_o - \tau^1) = \int_1^{\infty} e^{-(\tau_o - \tau^1)n} \frac{dn}{n^2} \tag{19}$$

therefore,

$$2B_v \int_1^{\infty} e^{-(\tau_o - \tau^1)n} \frac{dn}{n^2} = 2B_v E_{i2}(\tau_o - \tau^1) \tag{20}$$

The third exponential integral may also be written

$$E_{i3}(\tau_o - \tau^1) = \int_1^\infty e^{-(\tau_o - \tau^1)n} \frac{dn}{n^3} \tag{21}$$

Differentiating

$$2B_v E_{i2}(\tau_o - \tau^1) = -2B_v \frac{d}{d\tau}\left[E_{i3}(\tau_o - \tau^1)\right] \tag{22}$$

and

$$L^2{}_v(\tau_o) = -\int_{\tau_1}^{\tau_o} 2B_v \frac{d}{d\tau}\left[E_{i3}(\tau_o - \tau^1)\right] d\tau^1 \tag{23}$$

Since $B_v = \pi I_{bv}$ is the emitted flux density, $2E_{i3}(\tau_o - \tau^1)$ is the flux transmissivity which can be expressed as a function of optical depth $\psi^1(\tau_o - \tau^1)$ or of pathlength and temperature $\psi(u - u_o, T)$ where

$2E_{i3}(\tau_o - \tau^1) = \psi^1(\tau_o - \tau^1) = \psi(u - u_o, T)$. Therefore,

$$L^2{}_v(\tau_o) = -\int_{\tau_1}^{\tau_o} B_v \frac{d\psi}{d\tau}(u - u_o, T)\, d\tau \tag{24}$$

Since $\frac{d\psi}{d\tau}\, d\tau = \frac{d\psi}{du}\, du$

$$L^2(u_o) = -\int_{v_1}^{v_2} dv \int_{u_1}^{u_o} B_v \frac{d\psi}{du}(u - u_o, T)\, du \tag{25}$$

and the integration of wavenumber has been inserted.

The solution of the first term on the right hand side of equation (13) is obtained in a similar manner which gives

$$L^{1}(u_o) = \int_{v_1}^{v_2} \varepsilon_s B_v(\tau_1) \psi (u_1 - u_o, T) dv \qquad (26)$$

Combining equations (25) and (26) the incoming longwave flux density may now be expressed as

$$L(u_o) = \int_{v_1}^{v_2} \varepsilon_s B_v(\tau_1) \psi (u_1 - u_o, T) dv - \int_{v_1}^{v_2} \int_{u_1}^{u_o} B_v \frac{d\psi}{du} (u - u_o, T) du \qquad (27)$$

which defines L↓ under a cloud layer where τ_1 refers to the cloud base. For cloudless skies, the first term on the right hand side of equation (27) is zero and the spectral intensity of longwave irradiance becomes

$$L(u_o) = - \int_{v_1}^{v_2} dv \int_{u_1}^{u_o} B_v \frac{d\psi}{du} (u - u_o, T) du \qquad (28)$$

APPENDIX B

MEASURED LONGWAVE IRRADIANCE DATA USING THE EPPLEY SILICON-DOMED PYRGEOMETER (L_{SIL}) AND CALCULATED VALUES FROM FLUX EMISSIVITY MODELS EMPLOYING KUHN'S EMISSIVITIES (ELDOWN) AND STALEY AND JURICA'S EMISSIVITIES (SANDJ) FOR 1200Z and 2300Z ASCENTS. (Wm^{-2})

DATE	1200Z					2300Z				
	L_{SIL}	ELDOWN	DIFF(%)	SANDJ	DIFF(%)	L_{SIL}	ELDOWN	DIFF(%)	SANDJ	DIFF(%)
FEB. 19						201	186	-7	202	0
20	205	190	-7	202	-1					
27						206	215	+4	231	+12
28	193	205	+6	221	+15					
MAR. 16						248	215	-13	231	-7
17	251	223	-11	238	-5					
19						232	226	-3	245	+6
20	237	219	-8	233	-2	257	242	-6	260	+1
21						262	254	-3	271	+3
22	253	241	-5	255	+1	262	278	-6	296	+13
23	276	257	-7	273	-1					
APR. 10						226	207	-8	228	+1
11	229	201	-12	218	-5					
17						243	241	-1	260	+7
18	239	221	-8	238	0	245	240	-2	261	+7
19	237	209	-12	226	-5					
20						268	267	0	286	+7
21	269	257	-4	270	0					
MAY 17	269	239	-16	256	-5	243	273	+12	293	+21
18	267	268	0	285	+7	283	306	+8	327	+16
19	283	300	+6	319	+13					

DATE	1200Z					2300Z				
	L_{SIL}	ELDOWN	DIFF(%)	SANDJ	DIFF(%)	L_{SIL}	ELDOWN	DIFF(%)	SANDJ	DIFF(%)
JUNE 25						310	275	-11	297	-4
26	296	263	-11	280	-5					
AUG. 21	318	297	-7	314	-1	339	326	-4	348	+3
22	325	302	-7	318	-2					
OCT. 31	268	243	-9	255	-5					
NOV. 19	282	261	-7	274	-3					

*DIFF=% DIFFERENCE BETWEEN MEASURED AND MODEL IRRADIANCE. +INDICATES MODEL OVER-ESTIMATION
-INDICATES MODEL UNDER-ESTIMATION

APPENDIX C

MEASURED HOURLY IRRADIANCE DATA(Wm^{-2}) PLOTTED IN FIGURES 3-7

A. FIGURE 3: OCTOBER 31 (0100-1900)

time	L_{SIL}	L_{KRS-5}	L_{RES}	$K\downarrow$
0100	254	281	266	0
0200	257	281	268	0
0300	264	286	277	0
0400	262	287	275	0
0500	256	282	270	0
0600	266	288	279	0
0700	268	292	285	8
0800	274	304	289	64
0900	284	341	312	225
1000	291	353	310	363
1100	292	355	308	450
1200	293	363	304	478
1300	295	361	304	455
1400	291	341	308	363
1500	291	332	315	253
1600	292	331	321	114
1700	288	307	299	10
1800	287	309	299	0
1900	290	310	301	0

B. FIGURE 4: March 19 (1100-0000)

time	L_{SIL}	L_{KRS-5}	$K\downarrow$
1100	248	290	699
1200	252	295	716
1300	249	308	777
1400	246	291	705
1500	243	282	586
1600	234	280	401
1700	240	276	219
1800	239	258	35
1900	252	269	0
2000	252	268	0
2100	243	267	0
2200	234	259	0
2300	232	247	0
0000	237	251	0

C. FIGURE 5: APRIL 18 (0000-2300)

time	L_{SIL}	L_{RES}	$K\downarrow$
0000	240	247	0
0100	240	244	0
0200	237	241	0
0300	236	244	0
0400	235	240	0
0500	234	240	0
0600	233	260	27
0700	239	289	188
0800	253	285	390
0900	256	281	572
1000	268	290	728
1100	273	280	842
1200	286	286	900
1300	286	294	905
1400	281	296	832
1500	280	302	731
1600	280	322	571
1700	279	323	385
1800	266	307	185
1900	258	270	24
2000	250	245	0
2100	247	240	0
2200	245	242	0
2300	245	242	0

D. FIGURE 6: APRIL 11 (0000-1800)

time	L_{SIL}	L_{RES}	$K\downarrow$
0000	233	239	0
0100	226	232	0
0200	230	236	0
0300	214	218	0
0400	216	223	0
0500	214	218	0
0600	224	234	6
0700	229	252	95
0800	228	274	333
0900	242	281	504
1000	247	267	733
1100	261	262	864
1200	252	248	900
1300	265	271	581
1400	281	303	368
1500	291	313	273
1600	296	318	146
1700	302	323	84
1800	304	323	51

E. FIGURE 7: AUG. 23(1200)-AUG. 25(1000)

time	L(Q*)	L(Q↓)	K↓
1200	303	331	629
1300	310	330	684
1400	314	332	705
1500	320	319	618
1600	326	319	532
1700	324	319	412
1800	320	327	282
1900	326	318	152
2000	328	315	33
2100	297	288	0
2200	300	283	0
2300	296	285	0
0000	300	287	0
0100	298	282	0
0200	299	283	0
0300	298	284	0
0400	304	285	0
0500	304	285	0
0600	319	319	0
0700	321	339	87
0800	367	373	195
0900	316	326	336
1000	314	331	456
1100	309	313	564
1200	306	305	640
1300	317	311	673
1400	321	312	662
1500	318	309	618
1600	324	317	532
1700	328	313	423
1800	326	330	282
1900	329	326	152
2000	329	313	33
2100	298	289	0
2200	296	283	0
2300	292	281	0

time	L(Q*)	L(Q↓)	K↓
0000	290	278	0
0100	287	275	0
0200	283	273	0
0300	282	270	0
0400	285	272	0
0500	288	272	0
0600	287	282	0
0700	293	303	76
0800	314	318	184
0900	316	328	315
1000	311	320	434

*ALL L_{RES} AND L(Q↓) DATA WERE OBTAINED USING THE STYROFOAM MOUNTED PYRRADIOMETER.